

Hadronic top-quark pair production with NNLL threshold resummation

M. BENEKE^a, P. FALGARI^b, S. KLEIN^a, C. SCHWINN^c

^a*Institute für Theoretische Teilchenphysik und Kosmologie,
RWTH Aachen University, D-52056 Aachen, Germany*

^b*Institute for Theoretical Physics and Spinoza Institute,
Utrecht University, 3508 TD Utrecht, The Netherlands*

^c*Albert-Ludwigs Universität Freiburg, Physikalisches Institut,
D-79104 Freiburg, Germany*

Abstract

We compute the total top-quark pair production cross section at the Tevatron and LHC based on approximate NNLO results, and on the summation of threshold logarithms and Coulomb enhancements to all orders with next-to-next-to-leading logarithmic (NNLL) accuracy, including bound-state effects. We find

$$\sigma_{t\bar{t}}(\text{Tevatron}) = (7.22^{+0.31+0.71}_{-0.47-0.55}) \text{ pb}$$

$$\sigma_{t\bar{t}}(\text{LHC}, \sqrt{s} = 7 \text{ TeV}) = (162.6^{+7.4+15.4}_{-7.6-14.7}) \text{ pb}$$

for $m_t = 173.3 \text{ GeV}$. The implementation of joint soft and Coulomb resummation, its ambiguities, and the present theoretical uncertainty are discussed in detail. We further obtain new approximate results at N³LO.

1 Introduction

Fifteen years after the discovery of the top quark, the experimental uncertainty of the measurement of the top-pair production cross section at the Tevatron has dropped below ten percent [1–4]. At the LHC, the precision of the measurements quickly approaches that reached at the Tevatron [5, 6]. Therefore precision studies of the heaviest quark known today can be expected in the near future. An interesting use of the total cross section measurement is the extraction of the top-quark mass [7–9] in a cleaner (albeit less precise) way than the direct measurements. Furthermore, the total cross section provides constraints on new-physics models that try to explain the forward-backward asymmetry anomaly observed at CDF [10]. More generally, its experimental reconstruction involves several aspects, such as missing energy and b -quark tagging, relevant to the search for heavy particles in extensions of the Standard Model.

The precision of experiments motivates improving the accuracy of the theoretical calculation of the total top-pair production cross section beyond that of the next-to-leading order (NLO) result [11], and of the summation of leading-logarithmic (LL) or next-to-leading logarithmic (NLL) soft-gluon corrections [12–17]. Work on the complete next-to-next-to-leading order (NNLO) corrections is in progress and several ingredients are already known [18–27]. Meanwhile, progress in the understanding of the infrared structure of massive two-loop scattering amplitudes in QCD [28–33] has provided the prerequisites to compute soft-gluon effects at next-to-next-to-leading logarithmic (NNLL) accuracy [34–42].

In this paper we are concerned with resumming higher-order corrections to the partonic cross sections, $\hat{\sigma}_{pp'}$, for the processes

$$p(k_1)p'(k_2) \rightarrow t(p_1)\bar{t}(p_2) + X, \quad (1.1)$$

that become large in the partonic threshold limit,

$$\hat{s} \equiv (k_1 + k_2)^2 \rightarrow 4m_t^2, \quad (1.2)$$

where the top quarks have a small relative velocity $\beta = \sqrt{1 - \frac{4m_t^2}{\hat{s}}}$. In this limit corrections due to the radiation of soft gluons and the exchange of virtual Coulomb gluons are both enhanced, resulting in terms of the form $\alpha_s \log^{2,1} \beta$ and α_s/β at every order of the coupling expansion. Near the partonic threshold, $\beta \approx 0$, these corrections become large and should be resummed to all orders. Instead of organizing radiative corrections by the power of the strong coupling constant it is then appropriate to count both $\alpha_s \ln \beta$ and α_s/β as quantities of order one. Exploiting the exponentiation of double logarithmic terms leads to a parametric representation of the expansion of the cross section in the form

$$\begin{aligned} \hat{\sigma}_{pp'} &= \hat{\sigma}_{pp'}^{(0)} \sum_{k=0} \left(\frac{\alpha_s}{\beta} \right)^k \exp \left[\underbrace{\ln \beta g_0(\alpha_s \ln \beta)}_{\text{(LL)}} + \underbrace{g_1(\alpha_s \ln \beta)}_{\text{(NLL)}} + \underbrace{\alpha_s g_2(\alpha_s \ln \beta)}_{\text{(NNLL)}} + \dots \right] \\ &\times \{ 1 \text{ (LL,NLL)}; \alpha_s, \beta \text{ (NNLL)}; \alpha_s^2, \alpha_s \beta, \beta^2 \text{ (N}^3\text{LL)}; \dots \}. \end{aligned} \quad (1.3)$$

We remark that the structure of the expansion is significantly more complicated than for Drell-Yan or Higgs production. The presence of Coulomb enhancements, $(\alpha_s/\beta)^k$, not only calls for a joint summation of soft-gluon and Coulomb effects, but also implies that one must address $O(\beta)$ corrections from soft emission at NNLL [36, 39], which count as a power-suppressed effect in Drell-Yan and Higgs production. In general, increasing the order in (1.3) requires higher-loop corrections to anomalous dimensions to sum logarithms, and the inclusion of power corrections of increasingly higher order.

In order to obtain the total hadronic cross section, the partonic cross section is convoluted with the parton distribution functions. Both at Tevatron and LHC, the top anti-top invariant-mass distribution peaks at about 400 GeV, which corresponds (in the absence of radiation) to $\beta \approx 0.5$. The convolution of the partonic cross section with the parton luminosity is therefore dominated by the region $\beta > 0.3$, where the threshold approximation is not valid (see e.g [40]). Nevertheless, one often finds that the threshold expansion provides a reasonable approximation even outside its domain of validity. For instance, in the absence of the exact NLO calculation one would do much better including the threshold-enhanced NLO terms rather than staying with the LO approximation. In the same spirit, we consider NNLL threshold resummation, which includes the singular terms at threshold at NNLO as a subset, a useful step towards the full NNLO result. Even when the latter is finally known, the resummed result contains a set of higher-order terms that may shed light on the fixed-order expansion of the total cross section.

The resummation of threshold logarithms in top-pair production has been conventionally performed in Mellin-moment space [43, 44], and numerical results for resummed corrections [16, 45, 46] at NLL accuracy, or partial higher-order results obtained from expansions of the resummed cross section [17, 47], have been known for some time. In these works the Coulomb corrections were included in fixed order, which corresponds to setting $k = 0$ or 1 in (1.3). An approximate NNLO correction based on the expansion of the NNLL result up to order α_s^2 has been obtained in [36], while the effect of Coulomb corrections in the threshold region has been considered in [48, 49]. A combined resummation of soft and Coulomb corrections has not yet been performed, and will be done in this paper at NNLL accuracy. We employ the momentum-space approach to threshold resummation [50–52], and the next-to-leading order Coulomb Green function obtained in the context of top-quark production in electron-positron collisions [53, 54]. We include all corrections at NNLL accuracy defined by (1.3), apart from a class of higher-order non-relativistic (as opposed to soft) logarithms, whose summation would require an extension of results of [55, 56]. The fixed-order logarithmic correction at $\mathcal{O}(\alpha_s^2)$ was computed in [36] and is included in our results. The numerical impact of the resummation of these logarithms is expected to be in the per-mille range and their calculation is left for future work.

It should be mentioned that beyond the higher-order QCD effects discussed in our work, electroweak corrections and finite-width effects can become relevant at the level of precision aimed at by our NNLL resummation. The former have been computed in [57, 58] and are of the order of -2% for the total cross section at the LHC, and smaller at Tevatron, while the effect on distributions can be larger. Finite-width effects on the total cross section are expected to be of the order $\Gamma_t/m_t \lesssim 1\%$, as has been confirmed by recent calculations of

the NLO QCD corrections to the full $b\bar{b}W^+W^-$ final state [59,60].

Recently higher-order expansions and NNLL resummations in different kinematical variables, such as the invariant mass distribution and so called one-particle inclusive kinematics [37,38,41,42], became available. In these calculations different logarithms than the ones in the threshold expansion (1.3) are resummed. With respect to the total cross section, this amounts to including a particular set of higher-order terms in β , while excluding some of the more singular terms. Since the total cross section receives important contributions from outside the threshold region, the two resummation procedures are complementary. The numerical results of these studies appear to differ beyond the quoted uncertainties, which calls for particular attention to a realistic estimate of the remaining uncertainty inherent in the threshold expansion.

The paper is organized as follows. In Section 2 we review the combined soft and Coulomb resummation developed in [34,39] and provide the ingredients required to achieve NNLL resummation for top-quark pair production. We expand the NNLL resummed cross section to order α_s^3 and present a new result of exact terms beyond NNLO in Section 3. In Section 4 we discuss and define our implementation of resummation and the method to estimate the uncertainties resulting from the threshold approximation. Section 5 contains our final results for the top-quark pair production cross section at Tevatron and LHC for a range of top quark masses. Details of the evaluation of the NLO Coulomb correction, including the bound-state contribution, the complete expressions for the expansion up to order α_s^3 , and a discussion of our error estimate are contained in the appendices.

2 Basics of resummation

2.1 Summary of the resummation formula

Resummation of threshold logarithms is based on the factorization of the partonic cross section in the threshold region into several functions [43,61] receiving contributions from different kinematical regions (soft, hard, collinear...). The independence of the cross section on artificial scales introduced in this factorization implies evolution equations, whose solutions resum threshold logarithms to all orders. For the case of top pairs (and other heavy coloured particles) the situation is more complicated, since in the threshold region soft gluons and the non-relativistic top quarks have comparable energies of order $m_t\beta^2$, so that energy is modified by a relevant amount due to soft radiation. This is in contrast to the case usually considered in deriving factorization formulas at partonic thresholds, where all particles are taken to be highly energetic compared to the scale of the soft radiation. As a result, the factorization formula for the hard-scattering total cross section for the partonic subprocesses (1.1) near the partonic threshold (1.2) factorizes into three contributions [39], with a potential function J in addition to the hard and soft functions H and W :

$$\hat{\sigma}_{pp'}(\hat{s}, \mu) = \sum_{R=1,8} H_{pp'}^R(m_t, \mu) \int d\omega J_R(E - \frac{\omega}{2}) W^R(\omega, \mu). \quad (2.1)$$

Here $E = \sqrt{\hat{s}} - 2m_t$ is the energy relative to the production threshold. The sum is over the colour representations of the final state top-pair system, i.e. the colour-singlet and octet states. The hard functions H can be obtained from the colour-separated hard-scattering amplitudes for the process $pp' \rightarrow t\bar{t}$ in the threshold limit, as described in [39]. The soft function W^R is defined as a vacuum expectation value of soft Wilson lines, and can be reduced to one for a fictitious $2 \rightarrow 1$ scattering processes with a single final-state particle in the colour representation R , provided an appropriate s -channel colour basis is chosen [34]. Such a basis has been adopted in (2.1). The potential function J_R sums Coulomb gluon exchange related to the attractive or repulsive Coulomb force in the colour singlet and octet channels, respectively.

In the momentum-space approach [50–52] resummation is performed by evaluating the hard function $H(\mu)$ at a hard matching scale $\mu_h \sim 2m_t$ and the soft function $W(\omega, \mu)$ at a soft matching scale of the order of $\mu_s \sim m_t\beta^2$. Both are then evolved to an intermediate factorization scale μ_f using evolution equations. For the case of heavy pair production at threshold the relevant evolution equations and the solutions have been given in [34, 39], so we will only summarize the solutions below.

The convolution of the soft and potential functions in (2.1) accounts for the energy loss of the top pair into soft radiation. In our study of NLL resummation for squark anti-squark production [39] we observed a non-negligible numerical effect from the combined soft and Coulomb resummation, and also found a reduced scale dependence. For top anti-top production the Coulomb corrections are smaller, so we expect less sizeable effects for the case of top quarks.

The formula (2.1) has been derived in an effective field theory for the production of heavy particles in an S -wave state¹ and is valid for the leading effective Lagrangian. Corrections from subleading terms in the effective Lagrangian, or higher-dimensional production operators, potentially lead to the corrections $\mathcal{O}(\beta)$ (NNLL) and $\mathcal{O}(\alpha_s\beta, \beta^2)$ (N³LL) indicated in (1.3), and would have to be accounted for by including additional hard, potential and soft functions in (2.1). As shown in [36, 39], these subleading effects vanish at NNLL accuracy due to rotational invariance, so that the $\mathcal{O}(\beta)$ corrections are absent and factorization holds in the simpler form (2.1). Starting from N³LL order, such power-suppressed corrections in β should be expected, requiring the introduction of new soft and potential functions, as is also indicated by the massive two-loop soft anomalous dimension for non-threshold kinematics [31, 32], which exhibits a more complicated colour structure.

2.2 Inputs to the resummation formula

From (1.3) and the factorization formula (2.1), it can be seen that the ingredients required for NNLL resummation are given by the resummation functions in the exponent [39, 52],

¹Therefore the formula applies to the $q\bar{q}$ and gg initiated partonic channels but not to contributions from $qg, \bar{q}g$ initial states, that are suppressed by a factor β^2 and therefore formally of N³LL order. Results for the leading threshold-enhanced NNLO contributions for those channels have been given in [7].

the fixed-order one-loop soft [34] and hard [62] functions² and the NLO-resummed potential functions [53]. Once the only non-trivial process-dependent quantities, the one-loop hard functions, are known, the formalism can be immediately applied to perform an NNLL resummation for other processes, such as the production of coloured supersymmetric particles. In this subsection we collect the required ingredients.

2.2.1 Hard functions

The hard functions are related to the amplitudes of partonic top production processes $pp' \rightarrow t\bar{t}$ directly at threshold. Their perturbative expansion in the QCD coupling in the $\overline{\text{MS}}$ scheme can be written as

$$H_{pp'}^R(\mu_h) = H_{pp'}^{R(0)}(\mu_h) \left[1 + \frac{\alpha_s(\mu_h)}{4\pi} h_{pp'}^{R(1)}(\mu_h) + \mathcal{O}(\alpha_s^2) \right]. \quad (2.2)$$

The leading-order hard functions are related to the partonic Born cross section at threshold in the colour channel R , $\hat{\sigma}_{pp',R}^{(0)}$, according to

$$\hat{\sigma}_{pp',R}^{(0)}(\hat{s}) \underset{\hat{s} \rightarrow 4m_t^2}{\approx} \frac{\beta m_t^2}{2\pi} H_{pp'}^{R(0)}. \quad (2.3)$$

The NLO coefficients $h_{pp'}^R$ at the hard matching scale μ_h can be obtained by comparing the analytical result for the threshold expansion of the NLO top-pair cross section [62] to the NLO expansion of the resummed cross section [39]. Subtracting the NLO contribution from the Coulomb and soft function, we obtain

$$\begin{aligned} h_{q\bar{q}}^{\mathbf{8}(1)}(\mu_h) &= -2C_F \left[\ln^2 \left(\frac{\mu_h^2}{4m_t^2} \right) + 3 \ln \left(\frac{\mu_h^2}{4m_t^2} \right) - \frac{7\pi^2}{6} + 16 \right] \\ &\quad + \frac{2C_A}{3} \left[8 \ln \left(\frac{\mu_h^2}{4m_t^2} \right) + \frac{100}{3} - \frac{3\pi^2}{2} + 4 \ln 2 \right] - \frac{20}{3} \ln \left(\frac{\mu_h^2}{4m_t^2} \right) - \frac{44}{3}, \\ h_{gg}^{\mathbf{1}(1)}(\mu_h) &= -2C_A \left[\ln^2 \left(\frac{\mu_h^2}{4m_t^2} \right) - \frac{2\pi^2}{3} - 2 \right] + 2C_F \left(\frac{\pi^2}{2} - 10 \right), \\ h_{gg}^{\mathbf{8}(1)}(\mu_h) &= -2C_A \left[\ln^2 \left(\frac{\mu_h^2}{4m_t^2} \right) + \ln \left(\frac{\mu_h^2}{4m_t^2} \right) + \frac{5\pi^2}{12} + 4 \right] + 2C_F \left(\frac{\pi^2}{2} - 10 \right), \end{aligned} \quad (2.4)$$

in the $\overline{\text{MS}}$ scheme with five active quark flavours. Here $R = \mathbf{1}$ stands for the colour-singlet and $R = \mathbf{8}$ for the colour-octet channel, respectively. The colour factors are $C_A = N_C = 3$, $C_F = (N_C^2 - 1)/(2N_C) = 4/3$. While strictly speaking the leading term in the threshold expansion of the Born cross section appears in the hard function (2.3), in our numerical results below we use the exact expression for the Born cross section, that can be found e.g. in [45].

²The $\mathcal{O}(\alpha_s)$ constant contribution appearing at NNLL in (1.3) has been included in some earlier NLL predictions [16] in an approximate way.

The choice $\mu_h \approx 2m_t$ eliminates the logarithmic terms in the hard function at the matching scale, but the soft and Coulomb functions naturally live at parametrically smaller scales, of the order of $m_t\beta^2$ and $m_t\beta$, respectively. The solution to the renormalization group equation that sums logarithms of $\ln(\mu_h/\mu)$ is given by

$$H_{pp'}^R(\mu) = \exp[4S(\mu_h, \mu) - 2a_i^V(\mu_h, \mu)] \left(\frac{4m_t^2}{\mu_h^2} \right)^{-2a_\Gamma(\mu_h, \mu)} H_{pp'}^R(\mu_h), \quad (2.5)$$

with the functions S , a_i^V and a_Γ defined as [52]

$$\begin{aligned} S(\mu_h, \mu) &= - \int_{\alpha_s(\mu_h)}^{\alpha_s(\mu)} d\alpha_s \frac{\Gamma_{\text{cusp}}^r(\alpha_s) + \Gamma_{\text{cusp}}^{r'}(\alpha_s)}{2\beta(\alpha_s)} \int_{\alpha_s(\mu_h)}^{\alpha_s} \frac{d\alpha'_s}{\beta(\alpha'_s)}, \\ a_\Gamma(\mu_h, \mu) &= - \int_{\alpha_s(\mu_h)}^{\alpha_s(\mu)} d\alpha_s \frac{\Gamma_{\text{cusp}}^r(\alpha_s) + \Gamma_{\text{cusp}}^{r'}(\alpha_s)}{2\beta(\alpha_s)}, \\ a_i^V(\mu_h, \mu) &= - \int_{\alpha_s(\mu_h)}^{\alpha_s(\mu)} d\alpha_s \frac{\gamma_i^V(\alpha_s)}{\beta(\alpha_s)}. \end{aligned} \quad (2.6)$$

The labels r, r' denote the colour representation of the initial-state partons p, p' , while the label i refers to the colour of the initial-state partons and the representation R of the $t\bar{t}$ pair. Explicit results for the $\overline{\text{MS}}$ β -function, a_Γ and the Sudakov exponent S up to N³LL order can be found in [52]. The relevant anomalous dimension coefficients as needed for NNLL accuracy are collected in [34]. Starting from the two-loop order the evolution equation of the hard function is modified because of additional IR divergences, that are related to UV divergences of the potential function due to insertions of non-Coulomb potentials. In this work we will not consider these contributions (see end of section 2.2.3 below).

2.2.2 Soft functions

The resummed soft function in the momentum-space formalism [50–52] can be written as

$$W_i^{R,\text{res}}(\omega, \mu) = \exp[-4S(\mu_s, \mu) + 2a_{W,i}^R(\mu_s, \mu)] \tilde{s}_i^R(\partial_\eta, \mu_s) \frac{1}{\omega} \left(\frac{\omega}{\mu_s} \right)^{2\eta} \theta(\omega) \frac{e^{-2\gamma_E\eta}}{\Gamma(2\eta)}. \quad (2.7)$$

The auxiliary variable η is set to $\eta = 2a_\Gamma(\mu_s, \mu)$ after performing the derivatives. The function $a_{W,i}^R$ is defined, analogously to a_i^V in (2.6), in terms of the anomalous dimension $\gamma_{W,i}^R$, first obtained up to the two-loop level in [34]. The function $\tilde{s}_i^R(\rho)$ is the Laplace transform of the soft function. For resummation at NNLL accuracy we require the NLO soft function, which reads [34, 39]

$$\tilde{s}_i^R(\rho, \mu) = 1 + \frac{\alpha_s}{4\pi} \left[(C_r + C_{r'}) \left(\rho^2 + \frac{\pi^2}{6} \right) - 2C_R(\rho - 2) \right] + \mathcal{O}(\alpha_s^2), \quad (2.8)$$

where C_r is the quadratic Casimir operator in the colour representation r of the initial state parton p . As mentioned above, the soft matching scale μ_s should be chosen of the order $m_t\beta^2$ in order to resum large logarithms in the soft function. The precise choice we adopt in our numerical analysis will be discussed in Section 4.

2.2.3 The NLO Coulomb function

The potential function is related to the imaginary part of the zero-distance Coulomb Green function of the Schrödinger operator $-\vec{\nabla}^2/m_t - (-D_R)\alpha_s/r$. The coefficients of the Coulomb potential in the colour-singlet and colour-octet configuration are given by

$$D_1 = -C_F = -\frac{N_C^2 - 1}{2N_C}, \quad D_8 = -\left[C_F - \frac{C_A}{2}\right] = \frac{1}{2N_C}. \quad (2.9)$$

For NNLL resummation we require the Coulomb Green function up to next-to-leading order, which includes one insertion of the NLO Coulomb potential

$$\delta\tilde{V}(\mathbf{p}, \mathbf{q}) = \frac{4\pi D_R \alpha_s(\mu)}{\mathbf{q}^2} \frac{\alpha_s(\mu)}{4\pi} \left(a_1 - \beta_0 \ln \frac{\mathbf{q}^2}{\mu^2} \right), \quad (2.10)$$

where $\beta_0 = \frac{11}{3}C_A - \frac{4}{3}n_l T_f$ is the one-loop beta-function coefficient, and $a_1 = \frac{31}{9}C_A - \frac{20}{9}n_l T_f$. The insertion of $\delta\tilde{V}(\mathbf{p}, \mathbf{q})$ yields a factor $\alpha_s \times \alpha_s/\beta$, which according to (1.3) produces a NNLL correction. The potential function up to next-to-leading order can be written as

$$J_R(E) = 2 \text{Im} \left[G_{C,R}^{(0)}(0, 0; E) \Delta_{\text{nC}}(E) + G_{C,R}^{(1)}(0, 0; E) + \dots \right], \quad (2.11)$$

where $G_{C,R}^{(0)}$ is the solution to the Schrödinger equation with the leading Coulomb potential, resumming all $(\alpha_s/\beta)^n$ corrections, while $G_{C,R}^{(1)}$ sums $\alpha_s \times (\alpha_s/\beta)^n$ corrections by solving perturbatively the Schrödinger equation with one insertion of $\delta\tilde{V}(\mathbf{p}, \mathbf{q})$ [53]. The explicit expressions are given in Appendix A.

The NLO potential function is independent of the scale μ , though a residual scale dependence, formally of higher order, remains. We use a β -dependent scale [39],

$$\tilde{\mu}_C = \max\{2m_t\beta, C_F m_t \alpha_s(\tilde{\mu}_C)\}, \quad (2.12)$$

in the numerical evaluation. With this choice logarithms of β in the potential function arise only from the scale of the strong coupling. The lower limit in (2.12) is chosen to coincide with the Bohr scale of the lowest-lying bound state in the colour singlet channel, which is indeed the relevant scale for $\beta \rightarrow 0$ in this case, as can be seen from the argument of the logarithm in (A.5) below. There are no bound states in the repulsive colour-octet channel, but since the Coulomb effects are small in this case, the precise choice of scale is not important.

Further NNLL effects from the non-relativistic dynamics arise from NNLO terms in the heavy-quark potential not related to the Coulomb potential,

$$\delta\tilde{V}_{\text{NNLO}}(\mathbf{p}, \mathbf{q}) = \frac{4\pi D_R \alpha_s(\mu^2)}{\mathbf{q}^2} \left[\frac{\pi \alpha_s(\mu^2) |\mathbf{q}|}{4m} \left(\frac{D_R}{2} + C_A \right) + \frac{\mathbf{p}^2}{m^2} + \frac{\mathbf{q}^2}{m^2} v_{\text{spin}} \right], \quad (2.13)$$

where $v_{\text{spin}} = 0$ and $-2/3$ for a $t\bar{t}$ pair in a spin-singlet and spin-triplet state, respectively. The evaluation of an insertion of the non-Coulomb potential results in UV divergences that

cancel against IR divergences in the two-loop hard function, as mentioned in Section 2.2.1. After this cancellation a logarithm of β remains at NNLO, which counts as NNLL. The divergence also produces an additional contribution to the anomalous dimension γ_i^V of the hard function starting from the two-loop order. Since as mentioned above, we do not consider this additional contribution in the NNLL resummed hard function, the non-Coulomb corrections will be included only at fixed order in the number of non-relativistic logarithms. The corresponding NNLO correction for a final state in an arbitrary colour representation is given by [36]

$$\sigma_{X|\text{nC}} = \sigma_X^{(0)} \alpha_s^2(\mu) \ln \beta \left[-2D_R^2 (1 + v_{\text{spin}}) + D_R C_A \right]. \quad (2.14)$$

Here $\sigma_X^{(0)}$ is the Born cross section in the spin and colour channel X . For top quarks the Born cross section in the $q\bar{q}$ initiated channel is a pure colour-octet spin-triplet, whereas in gluon-gluon fusion the $t\bar{t}$ state is spin-singlet but colour-octet or singlet. In our numerical results, the corrections (2.14) are added to the potential function $J_R(E)$ in (2.11) through the factor³

$$\Delta_{\text{nC}}(E) = 1 + \alpha_s^2(\mu_C) \ln \beta \left[-2D_R^2 (1 + v_{\text{spin}}) + D_R C_A \right] \theta(E) \quad (2.15)$$

multiplying the leading Coulomb function $G_{C,R}^{(0)}(0, 0; E)$, with $\beta = (E/m_t)^{1/2}$. After convolution with the soft function this procedure yields the correct $\alpha_s^2 \ln \beta$ and $\alpha_s^3 \ln^3 \beta$ terms in the threshold expansion. The factorized form of the logarithmic non-Coulomb correction can be deduced from the results of [53] (given explicitly in the appendix of [56]) and [36], and produces correctly the series $\alpha_s^2 \log \beta \times (\alpha_s/\beta)^k$ of terms associated with the first non-Coulomb logarithm and any number k of Coulomb exchanges.

The non-relativistic anomalous dimension produces a series $\alpha_s \times (\alpha_s \log \beta)^n \times (\alpha_s/\beta)^k$, of which (2.15) is only the first term ($n = 1$, any k), that should also be summed for complete NNLL accuracy. This requires the generalization of results for top-quark pair production in e^+e^- collisions (see, e.g., [55, 56]) to the production of a colour-octet final state. The numerical effect of the leading non-Coulomb terms is an enhancement of the top production cross section of about 0.5% at Tevatron and LHC. The higher-order terms should therefore be very small, and we leave this resummation of non-relativistic logarithms to future work.

2.3 Calculation of the convolutions

The total hadronic cross section for the production of a $t\bar{t} + X$ final state in collisions of hadrons $N_{1,2}$ with centre-of-mass energy s is obtained from

$$\sigma_{N_1 N_2 \rightarrow t\bar{t} X}(s) = \sum_{p,p'=q,\bar{q},g} \int_{4m_t^2/s}^1 d\tau L_{pp'}(\tau, \mu_f) \hat{\sigma}_{pp'}(s\tau, \mu_f), \quad (2.16)$$

³For simplicity we implement the non-Coulomb correction factor only in the continuum, and not for the bound states, since the uncorrected bound-state effect is already very small; hence the theta-function in (2.15).

where the parton luminosity is defined in terms of the parton distributions functions (PDFs)

$$L_{pp'}(\tau, \mu) = \int_0^1 dx_1 dx_2 \delta(x_1 x_2 - \tau) f_{p/N_1}(x_1, \mu) f_{p'/N_2}(x_2, \mu). \quad (2.17)$$

We briefly discuss some technical issues encountered when performing the convolution of the resummed soft and potential functions in the partonic cross section (2.1), and the subsequent convolution with the parton luminosity.

We convolute the NLO Coulomb Green function (2.11) with the resummed soft function, including the (pseudo) bound-state contributions from energies below the nominal top anti-top threshold. We note that for integrated quantities, such as the total cross section, the top width can be set to zero in the Coulomb function. Thus, for the continuum contributions, the integral in (2.1) has to be evaluated for $0 < \omega < 2E$. The bound-state contributions are located at values $\omega_n > 2E$, and we discuss them in Appendix B. Here we focus on the continuum. For the relevant hierarchy of scales, $\mu_s < \mu_f$, the anomalous dimension η is negative and the expression (2.7) should be understood in the distributional sense [51].

Let us first discuss the simpler case where the non-Coulomb corrections to the potential function are neglected, i.e. $\Delta_{\text{nC}} = 1$ in (2.11). The convolution of the soft and potential functions in the factorization formula (2.1) is analytically continued to negative values of η according to

$$\begin{aligned} \int_0^{2E} d\omega J_R(E - \frac{\omega}{2}) \left[\frac{1}{\omega} \left(\frac{\omega}{\mu_s} \right)^{2\eta} \right]_* &= \int_0^{2E} \frac{d\omega}{\omega} \left[J_R(E - \frac{\omega}{2}) - J_R(E) + \frac{\omega}{2} J'_R(E) \right] \left(\frac{\omega}{\mu_s} \right)^{2\eta} \\ &+ \left[\frac{J_R(E)}{2\eta} - \frac{J'_R(E)E}{2\eta + 1} \right] \left(\frac{2E}{\mu_s} \right)^{2\eta}. \end{aligned} \quad (2.18)$$

The derivatives of the potential function appearing in (2.18) have been evaluated by expressing the hypergeometric function in terms of harmonic sums using methods from [63], as described in Appendix A. The double subtraction in (2.18) is sufficient to render the ω integral finite for $\eta > -1$. However, for $\eta < -1/2$ the convolution of the first term in the second-line square brackets with the parton luminosity in (2.16) requires regularization at the partonic threshold $\tau \rightarrow 4m_t^2/s \equiv \tau_0$, if the potential function is non-vanishing at $E = 0$, as is the case for the attractive colour-singlet Coulomb potential. To see this, note that in the region $\tau \sim \tau_0$ we can approximate $E = \sqrt{s\tau} - 2m_t \approx \frac{1}{2} \frac{s}{2m_t} (\tau - \tau_0)$. With $L_{pp'}(\tau, \mu_f)$ and $J(E)$ approaching constants as $\tau \rightarrow \tau_0$, the τ -integrand behaves as $(\tau - \tau_0)^{2\eta}$. Thus the τ -integral for the colour-singlet cross section is analytically continued to $\eta < -1/2$ according to

$$\begin{aligned} \int_{\tau_0}^1 d\tau L_{pp'}(\tau) J_1(E) \left(\frac{2E}{\mu_s} \right)^{2\eta} &= \frac{1}{2\eta + 1} L_{pp'}(\tau_0) J_1(0) (1 - \tau_0) \left(\frac{s - 4m_t^2}{2m_t \mu_s} \right)^{2\eta} \\ &+ \int_{\tau_0}^1 d\tau \left[L_{pp'}(\tau) J_1(E) \left(\frac{2E}{\mu_s} \right)^{2\eta} - L_{pp'}(\tau_0) J_1(0) \left(\frac{s\tau - 4m_t^2}{2m_t \mu_s} \right)^{2\eta} \right]. \end{aligned} \quad (2.19)$$

The pole at $\eta = -\frac{1}{2}$ in the first line cancels with the overall gamma function in the resummed soft function (2.7), so that the cross section (2.16) is now well-defined for $\eta > -1$. In order to avoid large numerical cancellations, it is practical to split the integration interval into two regions and perform the analytical continuation (2.19) only in a small region $\tau \in [\tau_0, \tau_0 + \Delta\tau]$. The potential function in the singlet channel at $E = 0$, $J_1(0)$, is given in (A.5). The derivative of the singlet potential function at $E = 0$ vanishes only at leading order so that further subtractions would be required when μ_s and μ_f are such that $\eta < -1$.

Alternatively, the left-hand side of (2.18) can be analytically continued to negative η by performing a partial integration with respect to ω . After one partial integration we obtain

$$\int_0^{2E} d\omega J_R(E - \frac{\omega}{2}) \left[\frac{1}{\omega} \left(\frac{\omega}{\mu_s} \right)^{2\eta} \right]_* = \frac{1}{2\eta} \left(\frac{2E}{\mu_s} \right)^{2\eta} J_R(0) - \frac{1}{2\eta} \int_0^{2E} d\omega \frac{dJ_R(E - \frac{\omega}{2})}{d\omega} \left(\frac{\omega}{\mu_s} \right)^{2\eta}. \quad (2.20)$$

The integral in the second line is well defined for $\eta > -1/2$. By applying a second partial integration, it can be continued to values $\eta > -1$, as in (2.18), generating boundary terms with derivatives of the Coulomb function. The boundary terms at $\omega = 0$ are zero in the analytic continuation from positive η . For those at $\omega = 2E$ only the singlet channel contributes, since the octet Coulomb function $J_8(0)$ and its derivatives at $E = 0$ vanish. The convolution of the boundary terms with the parton luminosity can be treated in the same way as the terms in the second line of (2.18), leading to expressions similar to (2.19). Note that for the LO Coulomb function only $J_1(0)$ is non-zero, whereas all higher derivatives vanish.

Including the non-Coulomb correction (2.15) in the potential function (2.11) makes the analytic continuation more complicated due to the additional term $J_R^{(0)}(E) \log(E/m_t)$, where $J_R^{(0)}(E) = \text{Im} [G_{C,R}^{(0)}(0, 0; E)]$. The octet case does not pose a problem, since the octet Coulomb function and its derivatives vanish faster than any power as $E \rightarrow 0$. But for the singlet $J_1^{(0)}(E) \ln(E/m_t)$ diverges in this limit, and we have to introduce an additional subtraction,

$$\int_0^{2E} d\omega J_1^{(0)}(E - \frac{\omega}{2}) \ln\left(\frac{E - \frac{\omega}{2}}{m_t}\right) \left[\frac{1}{\omega} \left(\frac{\omega}{\mu_s} \right)^{2\eta} \right]_* = J_1^{(0)}(0) \int_0^{2E} d\omega \ln\left(\frac{E - \frac{\omega}{2}}{m_t}\right) \frac{1}{\omega} \left(\frac{\omega}{\mu_s} \right)^{2\eta} + \int_0^{2E} d\omega \left(J_1^{(0)}(E - \frac{\omega}{2}) - J_1^{(0)}(0) \right) \ln\left(\frac{E - \frac{\omega}{2}}{m_t}\right) \frac{1}{\omega} \left(\frac{\omega}{\mu_s} \right)^{2\eta}. \quad (2.21)$$

The first integral on the right-hand side of (2.21) can be calculated analytically, whereas the second integral can be continued to lower values of η either using partial integration, as in (2.20), or as in (2.18), with the replacement $J_1(E) \rightarrow (J_1^{(0)}(E) - J_1^{(0)}(0)) \ln(E/m)$.

The convolution of the luminosity function $L_{pp'}(\tau)$ with the second integral on the right-hand side of (2.21) is finite, once the ω integration has been continued to negative

values of η . On the contrary, the first integral,

$$J_1^{(0)}(0) \int_0^{2E} d\omega \ln\left(\frac{E - \frac{\omega}{2}}{m_t}\right) \frac{1}{\omega} \left(\frac{\omega}{\mu_s}\right)^{2\eta} = \frac{J_1^{(0)}(0)}{2\eta} \left(\frac{2E}{\mu_s}\right)^{2\eta} \left\{ \ln\left(\frac{E}{m_t}\right) - \gamma_E - \psi(1 + 2\eta) \right\}, \quad (2.22)$$

contains a non-integrable singularity at $E = 0$ for $\eta < -1/2$. This can be subtracted and analytically continued to $\eta > -1$, similarly to (2.19).

3 Expansion to α_s^3

The expression for the resummed cross section (2.1) can be expanded to order α_s^n in the strong coupling, providing an approximation to the full $\mathcal{O}(\alpha_s^n)$ QCD calculation. The expansion of the NLL and NNLL resummed corrections up to order α_s^1 and α_s^2 , respectively, has been given in [36,39]. Here we provide the corresponding expansion of the NNLL result up to order α_s^3 . In this way, we generate the first terms in the threshold expansion of the third-order fixed-order cross section, whose size should be indicative of the quality of the fixed-order expansion. If there are no cancellations, integrating the threshold expansion gives a rough estimate of the correction that may be expected on top of the exact NNLO result, once it is known.

To generate the threshold expansion from the resummation formula, the scales have to be chosen as $\mu_s = k_s m_t \beta^2$, $\mu_C = k_C m_t \beta$, $\mu_h = k_h m_t$, where the k_X are numbers of order one. Those terms in the threshold expansion that are completely included at NNLL are independent of the k_X . The expansion of the resummation formula also includes terms that are beyond the NNLL accuracy, which may depend on the arbitrary constants k_X , and are presently not completely known. Adopting the notation

$$\hat{\sigma}_{pp',R}(\beta, \mu_f) = \hat{\sigma}_{pp',R}^{(0)} \left\{ 1 + \sum_n \sum_{m=0}^n \left(\frac{\alpha_s(\mu_f)}{4\pi} \right)^n f_{pp'(R)}^{(n,m)} \ln^m \left(\frac{\mu_f}{m_t} \right) \right\} \quad (3.1)$$

for the fixed-order expansion in the strong coupling of the partonic cross section in colour channel R , the result for the different production channels can be written as

$$\begin{aligned} f_{q\bar{q}(8)}^{(3,0)} &= 12945.4 \ln^6 \beta - 37369.1 \ln^5 \beta + 27721.4 \ln^4 \beta + 41839.4 \ln^3 \beta \\ &+ \frac{1}{\beta} [-2994.51 \ln^4 \beta + 2804.73 \ln^3 \beta + 3862.46 \ln^2 \beta - 6528.61 \ln \beta] \\ &+ \frac{1}{\beta^2} [153.93 \ln^2 \beta + 122.866 \ln \beta - 144.996] + \tilde{f}_{q\bar{q}(8)}^{(3,0)}, \end{aligned} \quad (3.2a)$$

$$\begin{aligned} f_{gg(1)}^{(3,0)} &= 147456. \ln^6 \beta - 59065.6 \ln^5 \beta - 286099. \ln^4 \beta + 349463. \ln^3 \beta \\ &+ \frac{1}{\beta} [121278. \ln^4 \beta + 103557. \ln^3 \beta - 164944. \ln^2 \beta + 56418.5 \ln \beta] \\ &+ \frac{1}{\beta^2} [22166. \ln^2 \beta + 39012.1 \ln \beta - 2876.61] + \tilde{f}_{gg(1)}^{(3,0)}, \end{aligned} \quad (3.2b)$$

$$\begin{aligned}
f_{gg(8)}^{(3,0)} &= 147456. \ln^6 \beta - 169658. \ln^5 \beta - 140834. \ln^4 \beta + 524210. \ln^3 \beta \\
&+ \frac{1}{\beta} [-15159.7 \ln^4 \beta - 5364.82 \ln^3 \beta + 19598.9 \ln^2 \beta - 17054.7 \ln \beta] \\
&+ \frac{1}{\beta^2} [346.343 \ln^2 \beta + 522.978 \ln \beta - 71.7884] + \tilde{f}_{gg(8)}^{(3,0)}. \tag{3.2c}
\end{aligned}$$

The terms given explicitly in (3.2) are those N³LO terms, which are predicted correctly by the NNLL approximation, and which belong to the NNLL terms according to (1.3). The remainder functions $\tilde{f}_i^{(3,0)}$, containing N³LL and higher-order terms, are collected in Appendix C, together with the coefficients of the $\ln(\mu_f/m_t)$ terms. There we also summarize the $\mathcal{O}(\alpha_s^2)$ terms from [36] and the k_X -dependent constants not given in [36], which are generated from the expansion of the NNLL resummation formula, but are formally beyond NNLL.

We note that while the Coulomb terms are generically $\mathcal{O}((\alpha_s/\beta)^n)$, there is no $1/\beta^3$ term at third order. Instead a bound-state contribution is present, that in the fixed-order expansion would appear as a $\delta(\beta)$ term, which is not included in (3.2) but can be deduced from the expressions given in Appendix B. The absence of a $1/\beta^3$ term implies that the convolution of the partonic cross section with the parton densities is still well-defined, since $d\hat{\sigma}_{pp'}/d\beta \propto \ln^2 \beta$ for small β . This ceases to be true at N⁴LO, where a $1/\beta^4$ term is present in $f_i^{(4,0)}$. At this order the fixed-order expansion of heavy particle pair production breaks down, and the summation of Coulomb terms is mandatory even for the total cross section, which is not necessarily threshold-dominated after the resummation has been implemented.

In order to judge the magnitude of the $\mathcal{O}(\alpha_s^3)$ -terms, we plot the corrections to the partonic cross section in Figures 1 and 2. We consider three approximations:

- $\Delta\text{NNLO}_{\text{app}}$, which consists of the singular terms of the $\mathcal{O}(\alpha_s^2)$ correction as $\beta \rightarrow 0$ [36].
- N^3LO_A , which adds to the above the $\mathcal{O}(\alpha_s^3)$ terms from (3.2), including the remainder functions.
- N^3LO_B , which adds to $\Delta\text{NNLO}_{\text{app}}$ the $\mathcal{O}(\alpha_s^3)$ terms from (3.2) with the remainder functions set to zero, i.e. the NNLL terms only.

The difference between the first and the other two approximations provides an estimate of the importance of the third-order terms, and hence the convergence of the fixed-order expansion. The difference between the two N³LO approximations represents an ambiguity in our estimate of the third-order terms.⁴

In the figures we plot the integrand of the convolution in the formula for the hadronic cross section (2.16), i.e. the product of the partonic cross section and the parton luminosity,

⁴For this estimate we choose $k_s = k_C = 1$ and $k_h = 2$, which differs from our canonical choice $k_s = k_C = k_h = 2$ discussed below. The reason for this is that the remainder functions turn out to be small for the canonical choice, so the difference between N^3LO_A and N^3LO_B would not provide a measure of the “natural” size of the sub-leading singular terms at N³LO.

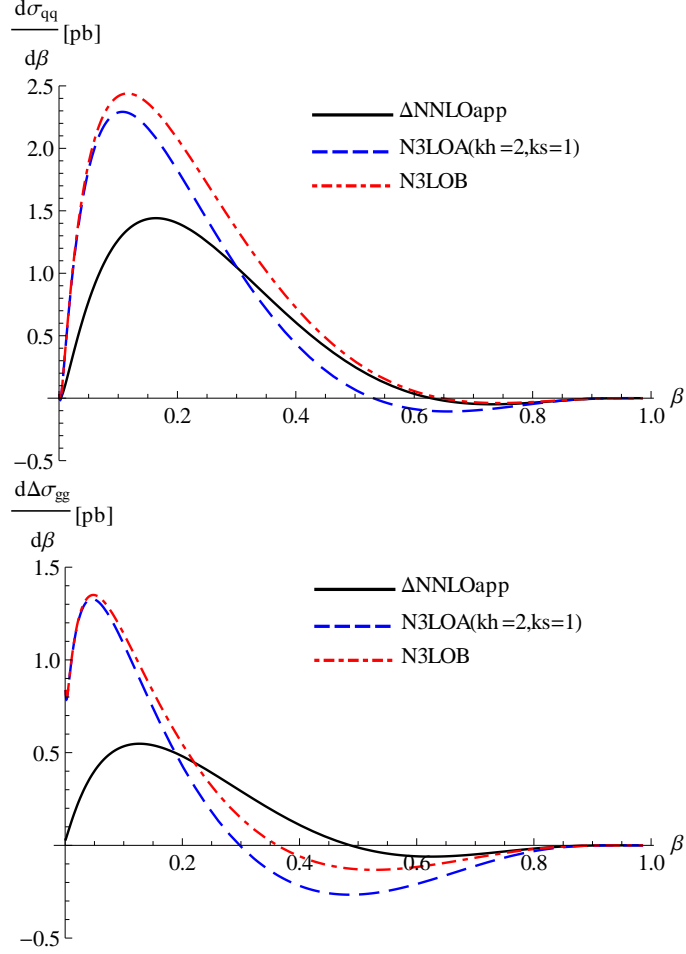


Figure 1: Partonic higher-order cross sections for $q\bar{q} \rightarrow t\bar{t}$ (top) and $gg \rightarrow t\bar{t}$ (below) at the Tevatron, multiplied with the parton luminosities. Black (solid): $\Delta\text{NNLO}_{\text{app}}$, blue (dashed): N^3LO_A (all terms in (3.2) for $k_s = k_C = 1$, $k_h = 2$), red (dot-dashed): N^3LO_B .

as a function of β , including the Jacobian $\partial\tau/\partial\beta$:

$$\frac{d\Delta\sigma_{pp' \rightarrow t\bar{t}}}{d\beta} = \frac{8\beta m_t^2}{s(1-\beta^2)^2} L_{pp'}(\beta, \mu_f) \Delta\hat{\sigma}_{pp' \rightarrow t\bar{t}}(\beta, \mu_f). \quad (3.3)$$

We show the partonic cross sections at the Tevatron (Figure 1) and LHC ($\sqrt{s} = 7 \text{ TeV}$, Figure 2), using the MSTW2008NNLO PDF set [64] and $\mu_f = m_t$. The third-order corrections are not negligible. The strong increase at small β should be expected, since for such small values of β the perturbative expansion breaks down and resummation should be performed. However, we note that for the gluon channel the magnitude of the third-order terms can be comparable to the second-order ones up to $\beta \approx 0.6$ (N^3LO_A). Unless there are cancellations with higher-order terms in the β expansion, which need not be small at $\beta \approx 0.5$, this may indicate a poor convergence of the fixed-order perturbative expansion.

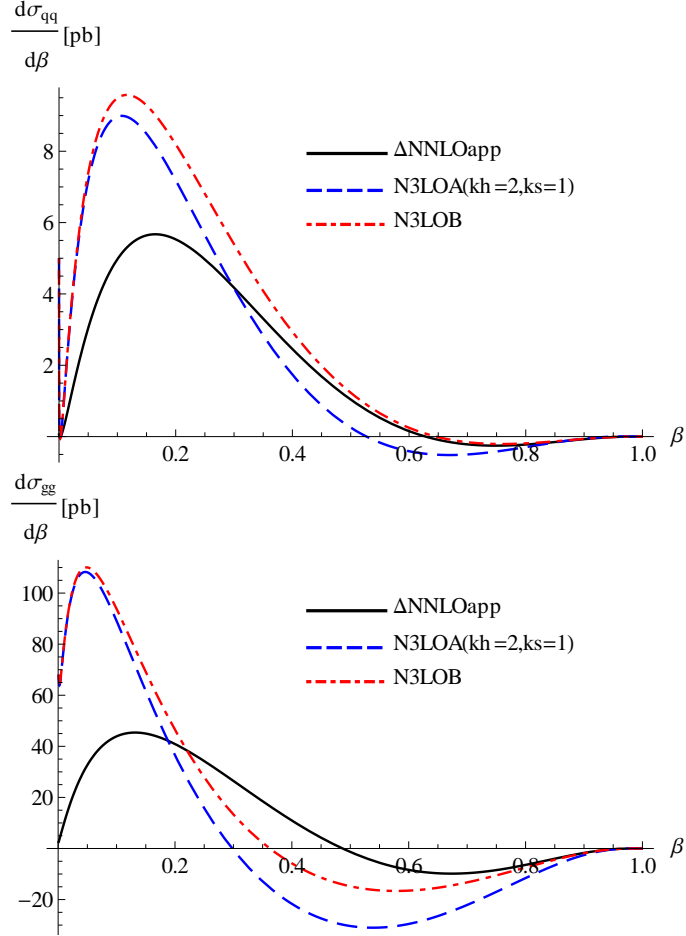


Figure 2: Partonic higher-order cross sections for $q\bar{q} \rightarrow t\bar{t}$ (top) and $gg \rightarrow t\bar{t}$ (below) at the LHC ($\sqrt{s} = 7$ TeV), multiplied with the parton luminosities. Black (solid): $\Delta\text{NNLO}_{\text{app}}$, blue (dashed): N^3LO_A (all terms in (3.2) for $k_s = k_C = 1$, $k_h = 2$), red (dot-dashed): N^3LO_B .

The area under the curves in the figures gives directly the correction to the total hadronic cross section that needs to be added to the NLO prediction. Adopting the top mass value $m_t = 173.3$ GeV, we obtain an additional 0.60 pb for $\Delta\text{NNLO}_{\text{app}}$, 0.93 pb (0.71 pb) for N^3LO_B (N^3LO_A) at the Tevatron and 12.1 pb for $\Delta\text{NNLO}_{\text{app}}$, 17.1 pb (7.8 pb) for N^3LO_B (N^3LO_A) at the LHC with $\sqrt{s} = 7$ TeV. The third-order term alone may therefore amount to up to 4% of the cross section at Tevatron and LHC. This might be considered as an estimate of the intrinsic uncertainty of the fixed-order prediction after the exact NNLO result is known. Below we shall see that resumming the threshold expansion to all orders in the NNLL approximation leads to a smaller effect from the sum of all higher-order terms.

4 Implementation of resummation and uncertainties

In the implementation of the resummation formalism one encounters several ambiguities: kinematical ambiguities, the precise matching to the fixed-order calculation, the choice of the scales μ_h and μ_s appearing in the momentum-space approach to threshold resummation, and the scale μ_C in the Coulomb function. We here discuss the choices made and the procedures to estimate the resulting theoretical uncertainties.

Kinematic ambiguities. If the total hadronic cross section (2.16) is computed by convoluting the factorized partonic cross section (2.1) with the parton luminosity for arbitrary values of τ , the application of the factorization formula is extended outside its domain of validity $\hat{s} \approx 4m_t^2$. As a result, there are kinematic ambiguities, since expressions that agree at partonic threshold can show numerical differences for $\beta \rightarrow 1$. One such ambiguity is related to the expression used for the hard function. As already mentioned in Section 2.2.1, we use the exact Born cross section, instead of the threshold limit, in the determination of the leading hard function (2.3), since this choice is observed to lead to a better agreement of the threshold approximation with the exact NLO result. Another ambiguity arises from the argument of the potential function J_R in (2.1). The derivation of the factorization formula [39] results in the dependence on the exact energy relative to the nominal production threshold, $E = \sqrt{\hat{s}} - 2m_t = 2m_t \times (1/\sqrt{1-\beta^2} - 1)$. However, the threshold expansion is customarily formulated as an expansion in β . In the threshold limit the two choices are equivalent, since $E \approx m_t\beta^2$, and hence one may replace E by $m_t\beta^2$ in the potential function. We have implemented both choices but use the second one as our default, since in this case the expansion parameter $E/m_t \rightarrow \beta^2$ is always smaller than 1, whereas it can grow to large values when the exact expression for E is used. The difference between the two implementations is used as a numerical estimate of the ambiguities in the resummation procedure.

Matching to the exact NLO result. Since the total production cross section is not numerically dominated by the threshold region, where the factorization formula (2.1) provides an accurate description of the cross section, we match the NNLL calculation to the exactly known NLO result. We consider two options. In the first, the NNLL cross section is expanded to NLO and subtracted from the resummed result. The resulting higher-order corrections are added to the full NLO result:

$$\hat{\sigma}_{pp',\text{matched},1}^{\text{NNLL}}(\hat{s}) = \left[\hat{\sigma}_{pp'}^{\text{NNLL}}(\hat{s}) - \hat{\sigma}_{pp'}^{\text{NNLL}(1)}(\hat{s}) \right] + \hat{\sigma}_{pp'}^{\text{NLO}}(\hat{s}). \quad (4.1)$$

This matching prescription will be denoted by NNLL₁ in the following. In this way, there is no double counting of $\mathcal{O}(\alpha_s)$ corrections. The expansion of the NNLL-resummed cross section to $\mathcal{O}(\alpha_s)$, $\hat{\sigma}_{pp'}^{\text{NNLL}(1)}$, coincides with the approximate NLO cross section given e.g. in (B.6) of [36]. For the NLO cross section we have implemented both the analytical result [65] and the parameterization given in [66]. For the former, we used the program provided in [67] for numeric evaluation.

The matched cross section (4.1) contains a constant term at NNLO, i.e. a β -independent correction multiplying the Born cross section. This includes the product of one-loop hard functions with the constant terms in the one-loop soft function (2.8), as well as terms related to ambiguities in the choice of the various scales. Since the two-loop hard and soft functions have not been computed yet, the constant NNLO term is not known completely, so the inclusion of a partial result is a matter of choice. We therefore consider a second matching option, denoted by NNLL₂, that matches to the NLO result by subtracting the expansion of the NNLL corrections to $\mathcal{O}(\alpha_s^2)$ and adding back the NNLO_{app} corrections: [36] with the unknown constant set to zero⁵

$$\hat{\sigma}_{pp',\text{matched},2}^{\text{NNLL}}(\hat{s}) = \left[\hat{\sigma}_{pp'}^{\text{NNLL}}(\hat{s}) - \hat{\sigma}_{pp'}^{\text{NNLL}(2)}(\hat{s}) \right] + \hat{\sigma}_{pp'}^{\text{NLO}}(\hat{s}) + \hat{\sigma}_{\text{app},pp'}^{\text{NNLO}}(\hat{s}). \quad (4.2)$$

The expansion of the NNLL correction to $\mathcal{O}(\alpha_s^2)$, $\hat{\sigma}_{pp'}^{\text{NNLL}(2)}$, is given in Appendix C. The numerical difference between the two implementations (4.1) and (4.2) can be considered as an estimate of the unknown constant term at NNLO. We discuss the issue of estimating the unknown constant further below.

For comparison, in the following we also present results for resummed cross sections with NLL accuracy. In addition to making the appropriate truncations for the resummation functions (2.6), in this approximation only the leading order terms in the soft (2.8) and hard function (2.2) are used, and the higher-order Green function $G_{C,R}^{(1)}$ and the non-Coulomb corrections Δ_{nC} are set to zero in the potential function (2.11). In contrast to the NNLL predictions, bound-state corrections will not be included in our NLL results presented in this paper. Here the two options to implement the matching are given by NLL₁, defined by

$$\hat{\sigma}_{pp',\text{matched},1}^{\text{NLL}}(\hat{s}) = \left[\hat{\sigma}_{pp'}^{\text{NLL}}(\hat{s}) - \hat{\sigma}_{pp'}^{\text{NLL}(0)}(\hat{s}) \right] + \hat{\sigma}_{pp'}^{\text{LO}}(\hat{s}), \quad (4.3)$$

and NLL₂, defined by

$$\hat{\sigma}_{pp',\text{matched},2}^{\text{NLL}}(\hat{s}) = \left[\hat{\sigma}_{pp'}^{\text{NLL}}(\hat{s}) - \hat{\sigma}_{pp'}^{\text{NLL}(1)}(\hat{s}) \right] + \hat{\sigma}_{pp'}^{\text{NLO}}(\hat{s}). \quad (4.4)$$

Because of our choice of the hard function, the expansion of the NLL correction to order α_s^0 , $\hat{\sigma}_{pp'}^{\text{NLL}(0)}$, coincides with the exact LO cross section $\hat{\sigma}_{pp'}^{\text{LO}}(\hat{s})$, so that $\hat{\sigma}_{pp',\text{matched},1}^{\text{NLL}}(\hat{s}) = \hat{\sigma}_{pp'}^{\text{NLL}}(\hat{s})$. The expansion of the NLL correction to $\mathcal{O}(\alpha_s^1)$, denoted by $\hat{\sigma}_{pp'}^{\text{NLL}(1)}$, is given in [39]. The NLL₂ matching is identical to the prescription used for squark-antisquark production in [39]. Since the full NLO corrections to top-pair production are known, this is the preferred implementation for phenomenological results, whereas the NLL₁ option is used to estimate ambiguities in the resummation procedure at NLL.

Unknown constant at $\mathcal{O}(\alpha_s^2)$. As mentioned in the previous paragraph, the constant term in the threshold approximation is unknown at $\mathcal{O}(\alpha_s^2)$. As a default, we do not include

⁵For consistency the constant terms are set to zero also in the coefficients $f_X^{(2,2)}$ and $f_X^{(2,1)}$ of the factorization-scale dependent terms, even though they are known in this case, see Appendix C.1.

such a constant in the results, unless it is generated by the resummation, as in the NNLL₁-option discussed below (4.1). However, we include an estimate of the order of magnitude of the constants in the determination of the uncertainty. Adopting the MSTW08NNLO PDFs, $\mu_f = m_t$ and $m_t = 173.3$ GeV, which is our standard choice, the numerical effect of non-vanishing constants for the different partonic channels is given by

$$\begin{aligned}
\text{Tevatron : } \Delta\sigma_{tt}^{(2)} &= \left[0.345 \left(\frac{C_{qq}^{(2)}}{1000} \right) + 0.024 \left(\frac{C_{gg,8}^{(2)}}{1000} \right) + 0.008 \left(\frac{C_{gg,1}^{(2)}}{1000} \right) \right] \text{ pb}, \\
\text{LHC}(\sqrt{s} = 7 \text{ TeV}) : \Delta\sigma_{tt}^{(2)} &= \left[1.70 \left(\frac{C_{qq}^{(2)}}{1000} \right) + 4.31 \left(\frac{C_{gg,8}^{(2)}}{1000} \right) + 1.31 \left(\frac{C_{gg,1}^{(2)}}{1000} \right) \right] \text{ pb}, \\
\text{LHC}(\sqrt{s} = 14 \text{ TeV}) : \Delta\sigma_{tt}^{(2)} &= \left[5.34 \left(\frac{C_{qq}^{(2)}}{1000} \right) + 27.14 \left(\frac{C_{gg,8}^{(2)}}{1000} \right) + 7.97 \left(\frac{C_{gg,1}^{(2)}}{1000} \right) \right] \text{ pb}.
\end{aligned} \tag{4.5}$$

Here our conventions are such that the correction to the partonic cross section due to the constant reads

$$\Delta\hat{\sigma}_{pp',R}^{(2)} = \hat{\sigma}_{pp',R}^{(0)} \left(\frac{\alpha_s}{4\pi} \right)^2 C_{pp',R}^{(2)}, \tag{4.6}$$

where $\hat{\sigma}_{pp',R}^{(0)}$ is the (exact) Born cross section for the pp' initial state in the colour channel R .

In order to get a crude estimate of the order of magnitude of the unknown $C_{pp',R}^{(2)}$, we consider the square of the corresponding one-loop constants. This method is observed to give a conservative estimate in cases where the full two-loop corrections are known. For top-pair production the one-loop constants have been calculated analytically [62]. In our conventions, they are related to the hard functions (2.4) by

$$C_{pp',R}^{(1)} = h_{pp'}^{R(1)}(m_t) + 4(C_r + C_{r'}) \left[9 \ln^2 2 - 12 \ln 2 + 8 - \frac{11\pi^2}{24} \right] - 12C_R [\ln 2 - 1]. \tag{4.7}$$

Numerically,

$$C_{q\bar{q}}^{(1)} = 14.531, \quad C_{gg,8}^{(1)} = 30.586, \quad C_{gg,1}^{(1)} = 14.026, \tag{4.8}$$

hence from $|C_{pp',R}^{(2)\text{est.}}| = (C_{pp',R}^{(1)})^2$ we obtain the estimates

$$|C_{qq}^{(2)\text{est.}}| = 211.2, \quad |C_{gg,8}^{(2)\text{est.}}| = 935.5, \quad |C_{gg,1}^{(2)\text{est.}}| = 196.7. \tag{4.9}$$

In our numerical results we estimate the uncertainty due to the unknown constant by adding and subtracting $|C_{pp',R}^{(2)\text{est.}}|$ in all partonic channels.

Choice of the soft scale. As discussed in Section 2, the resummation of threshold logarithms in the momentum-space approach amounts to resumming logarithms of the ratios μ_h/μ_f and μ_s/μ_f of the hard, soft and the factorization scale. While an all-order solution

to the evolution equations would be independent of these scales, a residual dependence remains after truncation of the perturbative series of the resummation functions S and a . Furthermore, the potential function depends on the Coulomb scale μ_C . Our default choices for the hard scale, $\mu_h = 2m_t$, and the Coulomb scale (2.12) have been explained in Section 2.2.

The proper choice of the soft scale requires some discussion. For any given β , the idea of scale separation in the effective theory suggests the β -dependent scale $\mu_s \sim m_t \beta^2$. Indeed, this choice has to be made to recover the threshold logarithms in fixed-order in α_s from the expansion of the resummed result. However, the use of a running scale in the resummed partonic cross section is problematic, since it leads to an oscillating partonic cross section for small values of β . The problem arises from $\eta = \frac{\alpha_s \Gamma_{\text{cusp}}}{2\pi} \log(\frac{\mu_s}{\mu_f}) + \dots$ becoming increasingly negative, such that the factor $1/\Gamma(2\eta)$ in (2.7) changes sign whenever a pole of the Gamma function is crossed. This effect appears in resummation for all hadron-collider processes such as Drell-Yan and Higgs production. In the traditional approach to threshold resummation in Mellin space, a similar difficulty appears when performing the inverse Mellin transform (see e.g. [13]), since the convolution of the resummed partonic cross section with the parton luminosity does not converge. The most widely used prescription to perform the convolution was proposed in [13], and amounts to performing the inverse Mellin transform at the level of the hadronic cross section. Other prescriptions have been suggested to perform the inverse Mellin transform directly for the partonic cross section but, in one way or another, employ a cutoff in the convolution with the parton luminosity, see e.g. [14, 68].

We investigate two methods to determine the soft scale: (1) a fixed soft scale determined according to a procedure proposed in [52] and (2) a running scale frozen to a fixed value below a certain value of β . In our final analysis we use the second method by default.

4.1 Method 1

In [50–52] it has been advocated to choose a fixed soft scale μ_s . In this approach one does not aim at predicting the partonic cross section locally as a function of β , but argues that logarithms in the *hadronic* cross section for $\tau_0 = 4m_t^2/s \rightarrow 1$ are resummed correctly by a fixed soft scale $\mu_s = 2m_t k_s (1 - \tau_0)$, where $k_s \sim 0.1$ due to the steeply falling parton luminosity function [52]. The partonic cross section is then predicted only in an average sense.⁶

In practice, the fixed soft scale is chosen such that it minimizes the relative fixed-order one-loop soft correction to the *hadronic* cross section. Following this procedure, we vary the scale in the PDFs and the soft correction and determine the value $\tilde{\mu}_s$ that minimizes the relative soft corrections:

$$0 = \tilde{\mu}_s \frac{d}{d\tilde{\mu}_s} \sum_{p,p'} \int_{4m_t^2/s}^1 d\tau L_{pp'}(\tau, \tilde{\mu}_s) \frac{\hat{\sigma}_{pp',\text{soft}}^{(1)}(\tau S, \tilde{\mu}_s)}{\sigma_{N_1 N_2}^{(0)}(s, \tilde{\mu}_s)}. \quad (4.10)$$

⁶See also [42] for a discussion of the differences between this approach and the use of fixed-order expansions.

Here the fixed-order NLO soft correction, $\hat{\sigma}_{pp'}^{(1)}$, is obtained from the threshold expansion of the NLO cross section (see e.g. (D.3) in [39]) by setting the Coulomb correction and the hard corrections h_i to zero. In the denominator we divide by the leading-order hadronic cross section.

In this approach the value of the soft scale depends on the interplay of coefficients of the logarithms and constants in the one-loop soft function (2.8), which might be considered as going against the philosophy of resumming only large logarithms. Furthermore, the reduction of the soft scale by a factor of 10 due to the behaviour of the PDFs compared to the naive expectation $\sim 2m_t(1 - \tau_0)$, has been estimated [52] to be effective for $\tau_0 > 0.2$, while for $\tau_0 \rightarrow 0$ the relevant soft scale is expected to be of the order $\mu_s \sim m_t$. For top-quark production at the Tevatron and the LHC with centre-of-mass energies up to 14 TeV the relevant range is $\tau_0 = 0.03 - 6 \times 10^{-4}$, so it cannot be expected *a priori* that the effect of the higher-order $\log \beta$ terms in the partonic cross section can be properly incorporated in an average sense through a fixed μ_s .

As discussed previously, there is a kinematic ambiguity from expressing the one-loop soft corrections in terms of $\log(E/\mu_s)$ or of $\log(m_t\beta^2/\mu_s)$. For a process dominated by threshold dynamics, the effect of this ambiguity on the soft scale determined through (4.10) should be small. However, for the case of top-quark production, we obtain noticeable differences between the soft scales determined using the two parameterizations of the soft function:

$$\begin{aligned} \log(E/\mu_s) : \quad & \tilde{\mu}_s = 52 \text{ GeV (Tevatron)}, \quad 99 \text{ GeV (LHC7)}, \quad 120 \text{ GeV (LHC14)}, \\ \log(m_t\beta^2/\mu_s) : \quad & \tilde{\mu}_s = 35 \text{ GeV (Tevatron)}, \quad 58 \text{ GeV (LHC7)}, \quad 65 \text{ GeV (LHC14)}. \end{aligned} \quad (4.11)$$

This difference, up to a factor of almost two, is a result of the fact that the total cross section is dominated by values $\beta \gtrsim 0.3$, and is another hint that the use of a fixed soft scale is somewhat problematic for top quark production.⁷

We nevertheless present results obtained using a fixed soft scale, in order to discuss the numerical impact of the potential problems in practice. We show numbers for both the (N)NLL₁ and (N)NLL₂ matching prescriptions, and use $E \rightarrow m_t\beta^2$. Note that for a fixed soft scale not all the logarithms of β are resummed locally in the partonic cross section, so the implementations (N)NLL₁ and (N)NLL₂ differ not only by a constant but also by logarithmic terms at $\mathcal{O}(\alpha_s^2)$. The soft scale is chosen as in the second line of (4.11). For the factorization scale we take $\tilde{\mu}_f = m_t$, for the hard scale $\tilde{\mu}_h = 2m_t$, as discussed in Section 2.2.1. The Coulomb scale $\tilde{\mu}_C$ is defined in (2.12). We estimate the theoretical uncertainty as follows:

Scale uncertainty: We vary all scales μ_i (the factorization, soft, hard and Coulomb scales) in the interval $[\tilde{\mu}_i/2, 2\tilde{\mu}_i]$ around their central values $\tilde{\mu}_i$. μ_s and μ_C are varied while keeping the other scales fixed. μ_h and μ_f are allowed to vary simultaneously,

⁷For the production of heavier particles, where the threshold region is more important, this ambiguity is indeed smaller. For instance, for $m_t = 1 \text{ TeV}$ and the LHC with $\sqrt{s} = 7 \text{ TeV}$ we find $\tilde{\mu}_s = 188 \text{ GeV}$ expressing the soft function in terms of $\log(E/\mu_s)$, and $\tilde{\mu}_s = 149 \text{ GeV}$ using $\log(m_t\beta^2/\mu_s)$, so the difference is reduced to less than 30%.

	Tevatron	LHC ($\sqrt{s} = 7$ TeV)	LHC ($\sqrt{s} = 14$ TeV)
NLL ₁	6.60 ^{+0.43 +0.00 +0.10 +0.50} _{-0.65 -0.61 -0.10 -0.44}	129.9 ^{+26.3 +0.00 +4.7 +10.2} _{-30.2 -15.6 -4.7 -9.7}	692 ^{+169 + 0 +28 +46} _{-180 -85 -28 -41}
NLL ₂	6.90 ^{+0.32 +0.00 +0.10 +0.52} _{-0.41 -0.04 -0.10 -0.47}	157.6 ^{+23.2 +2.3 +4.7 +13.5} _{-20.2 -0.00 -4.7 -12.8}	876 ^{+135 +14 +28 +64} _{-113 - 0 -28 -56}
NNLL ₁	6.87 ^{+0.31 +0.00 +0.10 +0.65} _{-0.40 -0.02 -0.10 -0.50}	151.8 ^{+9.4 +5.5 +4.7 +13.7} _{-4.9 -0.0 -4.7 -13.2}	837 ^{+69 +36 +28 +57} _{-28 - 0 -28 -57}
NNLL ₂	7.08 ^{+0.15 +0.07 +0.10 +0.69} _{-0.28 -0.00 -0.10 -0.53}	157.4 ^{+8.8 +5.4 +4.7 +14.5} _{-3.6 -0.0 -4.7 -13.9}	868 ^{+63 +29 +28 +61} _{-21 - 0 -28 -60}

Table 1: Results for Method 1, $m_t = 173.3$ GeV, all numbers in pb. The four errors refer to scale variation, resummation ambiguity, the NNLO constant term, and the PDF+ α_s uncertainty.

imposing the additional constraint $1 \leq \mu_h/\mu_f \leq 4$. The errors from varying $\{\mu_f, \mu_h\}$, μ_s and μ_C are obtained by taking the respective maximum/minimum, and are added in quadrature.

Resummation ambiguities: We estimate ambiguities in the resummation procedure by taking the difference between the default $E \rightarrow m_t\beta^2$ and $E = \sqrt{s} - 2m_t$. With the second expression for E the soft scales in the first line of (4.11) are used.

NNLO-constant: All constants $C_{pp',R}^{(2)}$ in (4.5) are varied by $\pm|C_{pp',R}^{(2)\text{est.}}|$.

PDF+ α_s uncertainty: We estimate the combined error of the NNLL results due to uncertainties in the PDFs and the strong coupling using the 90% confidence level eigenvector set of the MSTW08NNLO PDFs [64] and the five sets for variations of α_s provided in [69], which corresponds to $\alpha_s(M_Z) = 0.1171 \pm 0.0034$. For the NLL prediction the corresponding NLO PDFs are used.

For the top quark pole mass $m_t = 173.3$ GeV, we obtain the total top pair production cross sections displayed in Table 1, where the four errors refer to the four sources of uncertainty detailed above. Both, at the NLL and NNLL order, the central values for the two matching procedures lie inside the common error band. The total relative theory error, given by the sum in quadrature of the scale, resummation and constant uncertainties, decreases from NLL to NNLL, as one would expect from including higher orders in the logarithmic expansion, and increases from Tevatron to LHC, consistent with the fact that the threshold kinematics is parametrically more dominant at Tevatron, and thus matching and resummation ambiguities are expected to be smaller.

The difference of the NLL₁ results, both to the NNLL₁ and the complete fixed-order NLO predictions, (see Tables 8 and 10 in Section 5) are large, especially at the LHC, since in NLL₁ the fixed-order NLO corrections are not included through matching. The difference between NLL₂ and the fixed order NLO results, as well as the two NNLL implementations, is small in comparison. Since part of the difference is due to the use of different PDFs (NLO

vs. NNLO), it is instructive to compare predictions using NNLO PDFs also at NLL in order to ascertain the genuine effect of the higher-order corrections. For the NLL₂ approximation we then find the central values $\sigma_{t\bar{t}}^{\text{NLL}_2} = 6.67$ pb at the Tevatron and $\sigma_{t\bar{t}}^{\text{NLL}_2} = 148.6$ pb at the LHC with $\sqrt{s} = 7$ TeV ($\sigma_{t\bar{t}}^{\text{NLL}_2} = 830$ pb with $\sqrt{s} = 14$ TeV). Since in both the NLL₂ and NNLL₁ prescriptions the resummed cross section is matched to the fixed-order NLO result, their difference shows that the genuine effect of going from NLL to NNLL is moderate, and leads to an enhancement of about 3% at the Tevatron and below 1% at the LHC with $\sqrt{s} = 14$ TeV. The difference of the two NNLL implementations is of the order of 3 – 4%, and is an estimate for the effect of the constant terms at NNLO and the difference of including all $\log \beta$ terms exactly at NNLO or approximately due to the use of a fixed μ_s .

The total error, obtained by summing in quadrature the four sources of uncertainty, is dominated by the scale uncertainty and the error associated with PDF and α_s variation. Despite the ambiguity in the determination of the soft scale (4.11), the error associated to resummation is small at both Tevatron and LHC. The scale uncertainty decreases from NLL to NNLL, and is systematically smaller for the second matching option compared to the first.

4.2 Method 2

For the reasons explained in Section 4.1, the use of a fixed soft scale may be problematic for top-quark production at the Tevatron or LHC, where the total cross section is not dominated by the threshold region, but where it is nevertheless useful to include logarithmic higher-order corrections. We therefore propose a procedure that uses a running scale and fixes the soft scale only in the low- β region. We divide the convolution of the partonic cross section with the parton luminosity (2.16) into two regions using a parameter β_{cut} , chosen such that on the one hand the perturbative expansion in α_s is not spoiled by large logarithms in the upper interval $\beta > \beta_{\text{cut}}$, and on the other hand ambiguities in the threshold approximation are small in the lower interval $\beta < \beta_{\text{cut}}$. The partonic cross section is then treated differently in the two regions:

$\beta < \beta_{\text{cut}}$ For β_{cut} chosen sufficiently small (say $\beta_{\text{cut}} < 0.5$) the threshold expansion in β is convergent in the lower interval and the use of the factorization formula (2.1) is justified. In this region, the logarithms of β become large and need to be resummed for a reliable prediction. The threshold-enhanced contributions are numerically dominant and ambiguities in the resummation procedure, like the kinematical ambiguities or the use of the different matching prescriptions (4.1) and (4.2), should not lead to large numerical differences. For the reasons discussed before we use the NNLL₂ implementation defined in (4.2), with $E \rightarrow m_t \beta^2$ and a fixed soft scale

$$\mu_s^< = k_s m_t \beta_{\text{cut}}^2. \quad (4.12)$$

The choice of the constant k_s is discussed below.

$\beta > \beta_{\text{cut}}$ In the upper interval, the use of the threshold approximation cannot be justified a priori. Nevertheless we here adopt the point of view that the inclusion of a subset of higher-order corrections is useful even in this region. For β_{cut} chosen large enough, so that the perturbative expansion is not spoiled by large logarithms, the numerical difference of the NNLL resummed cross section and the expansion to NNLO and N³LO accuracy is expected to be small, so that the result should not depend too strongly on the choice of one of these approximations. By default we use again the implementation NNLL₂ with $E \rightarrow m_t \beta^2$. Since for $\beta \rightarrow 1$ it is not possible to argue that a fixed soft scale correctly includes dominant contributions to the hadronic cross section, we choose a running soft scale,

$$\mu_s^> = k_s m_t \beta^2, \quad (4.13)$$

in order to include all NNLL contributions to the *partonic* cross section correctly. In order to estimate the ambiguities in this treatment, we compare it to the approximate fixed-order cross sections NNLO_{app} [36], as well as N³LO_A and N³LO_B defined in Section 3, in each case including all lower-order terms up to the indicated order.

There is a certain tension in the requirements on β_{cut} . If chosen too large, the cross section result becomes too sensitive to the ambiguities in the matching procedure and the resulting constant terms at $\mathcal{O}(\alpha_s^2)$. Furthermore, a larger β_{cut} implies a larger $\mu_s^<$, so that resummation becomes ineffective. On the other hand, for β_{cut} too small the difference among successive orders in the perturbative expansion in the upper interval becomes too large (c.f. Figure 1). This suggests the following procedure to determine β_{cut} : we consider the cross section

$$\hat{\sigma}_{t\bar{t}}(A_<, B_>, \beta_{\text{cut}}) = \hat{\sigma}_{t\bar{t}}^{A_<} \theta(\beta_{\text{cut}} - \beta) + \hat{\sigma}_{t\bar{t}}^{B_>} \theta(\beta - \beta_{\text{cut}}), \quad (4.14)$$

defined using one of the appropriate approximations for the upper and lower intervals, $A_< \in \{\text{NNLL}_1, \text{NNLL}_2\}$ and $B_> \in \{\text{NNLL}_2, \text{NNLO}_{\text{app}}, \text{N}^3\text{LO}_A, \text{N}^3\text{LO}_B\}$, and determine β_{cut} such that the difference between the eight different implementations $\hat{\sigma}_{t\bar{t}}(A_<, B_>, \beta_{\text{cut}})$ becomes minimal.

We repeat this procedure for values $k_s = 1, 2, 4$ in the soft scales (4.12) and (4.13) in the two intervals. As default we adopt $k_s = 2$, and obtain the following values for β_{cut} and the corresponding fixed soft scale in the lower interval:

$$\begin{aligned} \beta_{\text{cut}}(\text{NNLL}) : & \quad 0.35 (\text{Tevatron}), & \quad 0.54 (\text{LHC7}), & \quad 0.55 (\text{LHC14}), \\ \mu_s^< = 2m_t \beta_{\text{cut}}^2 : & \quad 42 \text{ GeV} (\text{Tevatron}), & \quad 101 \text{ GeV} (\text{LHC7}), & \quad 105 \text{ GeV} (\text{LHC14}). \end{aligned} \quad (4.15)$$

It is seen that the β_{cut} values are in a region where we expect the β -expansion and the perturbative expansion in α_s both to be reasonably reliable, so they satisfy the requirements discussed above. We treat the difference to the results for $k_s = 1, 4$ as another source of the theoretical uncertainty. More details on this procedure and the β_{cut} values for $k_s = 1, 4$ are given in Appendix D.

To summarize, our default implementation is given by the option NNLL₂ defined in (4.2) using the soft scales (4.12) and (4.13), with $k_s = 2$ in both intervals and the β_{cut} -values given

	Tevatron	LHC ($\sqrt{s} = 7$ TeV)	LHC ($\sqrt{s} = 14$ TeV)
NLL ₂	7.31 ^{+0.25 +0.30 +0.10 +0.57} _{-0.03 -0.53 -0.10 -0.54}	172.8 ^{+14.8 +13.0 +4.7 +15.9} _{- 0.8 -14.7 -4.7 -14.6}	954 ^{+85 +65 +28 +74} _{- 5 -71 -28 -66}
NNLL ₂	7.22 ^{+0.21 +0.20 +0.10 +0.71} _{-0.41 -0.21 -0.10 -0.55}	162.6 ^{+4.2 +3.9 +4.7 +15.4} _{-1.9 -5.6 -4.7 -14.7}	896 ^{+22 +18 +28 +65} _{- 5 -23 -28 -64}

Table 2: Results for Method 2, $m_t = 173.3$ GeV, all numbers in pb. The four errors refer to scale variation, resummation ambiguity, the NNLO constant term, and the PDF+ α_s uncertainty.

in (4.15). For the remaining scales we again take the default values $\tilde{\mu}_f = m_t$, $\tilde{\mu}_h = 2m_t$ and the Coulomb scale as defined in (2.12). We estimate the remaining uncertainties as following:

Scale uncertainty: as for Method 1, excluding the soft scale. The latter is effectively replaced by the variation of k_s .

Resummation ambiguities: we consider three different sources for ambiguities: i) The difference between the default setting $E = m_t\beta^2$ compared to $E = \sqrt{\hat{s}} - 2m_t$ in the NNLL₂ implementation, ii) the difference between the NNLL₂ implementation for the soft scale choices $k_s = 1, 4$ (and the corresponding β_{cut} values) to the default choice $k_s = 2$, iii) the envelope of the 8-different approximations (4.14) for variations of β_{cut} by 20% around the default values (4.15) for $k_s = 2$. The resulting errors are added in quadrature.

NNLO-constant, PDF+ α_s uncertainty: estimated as in Method 1.

Our results for Method 2 are shown in Table 2, where the four errors refer to the four sources of uncertainty as detailed above. The separate sources of resummation ambiguity are shown in more detail in Table 3, from which one can see that the variation of k_s and β_{cut} (i.e. the soft-scale variation) dominate the error, while the ambiguity due to the use of $E = m_t\beta^2$ is negligible. To see the genuine effect of NNLL resummation it is again useful to consider the NLL₂ results using the NNLO PDFs for which we obtain $\sigma_{t\bar{t}}^{\text{NLL}_2} = 7.02$ pb at the Tevatron and $\sigma_{t\bar{t}}^{\text{NLL}_2} = 162.2$ pb at the LHC with $\sqrt{s} = 7$ TeV ($\sigma_{t\bar{t}}^{\text{NLL}_2} = 901$ pb at the LHC with $\sqrt{s} = 14$ TeV). Therefore the effect of the NNLL corrections on the central values is small, about 3% at the Tevatron and in the per-mille range at the LHC, showing a good convergence of successive orders of the logarithmic approximations.

The NNLL₂ results in Table 2 are about 3% larger than those obtained in Table 1 using Method 1, while for the NLL₂ results the differences are of the order of 10%. However the results from the two methods agree within the estimated resummation ambiguity. Since the soft scales corresponding to β_{cut} in (4.15) lie in the range of the fixed soft scales used for Method 1 (4.11), the differences between the two methods are smaller than might have been expected, and serve as an estimate of the effect of treating logarithmic corrections exactly for large β , as in Method 2, or approximately through a fixed soft scale, as in

Collider	i) E		ii) k_s		iii) β_{cut}	
Tevatron	+0.01 -0.00	{+0.1%} {-0.0%}	+0.10 -0.10	{+1.4%} {-1.4%}	+0.17 -0.18	{+2.4%} {-2.5%}
LHC ($\sqrt{s} = 7$ TeV)	+1.0 -0.0	{+0.6%} {-0.0%}	+0.8 -2.2	{+0.5%} {-1.4%}	+3.7 -5.1	{+2.3%} {-3.1%}
LHC ($\sqrt{s} = 14$ TeV)	+5 -0	{+0.6%} {-0.0%}	+ 0 -10	{+0.0%} {-1.1%}	+17 -21	{+1.9%} {-2.3%}

Table 3: Different resummation ambiguities of the NNLL₂ cross section for $m_t = 173.3$ GeV. Absolute errors are in pb. Relative errors are given in brackets.

Method 1. Since the results of both (very different) methods for the treatment of the soft scale agree within errors, we are confident that we are realistically estimating the resummation ambiguities.

The total relative theoretical error (not including the PDF+ α_s uncertainty) is shown in Table 4 for the NLL₂ and NNLL₂ cross sections, and for the NNLO_{app} result (see Section 5, Tables 8 and 10, for the absolute values). Both for the Tevatron and the LHC, the theoretical error decreases when higher-order logarithmic corrections are added to NLL₂. However at the Tevatron the smallest uncertainty is obtained for NNLO_{app}, while NNLL₂ yields the smallest error estimate for LHC. To understand this somewhat surprising behaviour at the Tevatron, in Table 5 we study separately the results for the quark-antiquark and gluon-gluon channels. It is seen that the increase of the error estimate for the quark-antiquark induced channel from NNLO_{app} to NNLL₂ occurs both at the Tevatron and the LHC. On the contrary, at the LHC the error of the dominant gluon channel is reduced at NNLL₂, which leads to the observed reduction of the total theoretical uncertainty. At the Tevatron a reduction of the error in the gluon channel is observed as well, if the same value $\beta_{\text{cut}} = 0.54$ as for LHC is used.⁸ It is interesting to recall that a comparison of the NLO singular terms with the exact NLO results (see e.g. [38, 39]) shows that, while the exact partonic cross section for the gg channel is approximated reasonably well by its threshold approximation over the whole β range, for the $q\bar{q}$ channel the approximation breaks down at $\beta \sim 0.3$. This points to a more problematic behaviour of the quark-antiquark channel. Therefore one might conclude that the small error of the NNLO_{app} prediction at the Tevatron is an underestimate of the true uncertainty, due to the particular behaviour of the dominant quark-antiquark channel.⁹

To summarize, by using a running soft scale within Method 2, we implement the principle of scale separation in effective theories at the level of the partonic cross section, rather

⁸This observation could suggest a separate β_{cut} choice for both channels, however due to the small effect on the central value we continue to use the same values.

⁹Another indication of this comes from a study of the choice $\tilde{\mu}_r = 2m_t$ for the central value of the renormalization scale in NNLO_{app}, that is identical to the central value of μ_h in the NNLL results. For this choice, the scale-uncertainty increases moderately to $^{+7.3\%}_{-8.2\%}$ for NNLO_{app} at the LHC with $\sqrt{s} = 7$ TeV, while the error at the Tevatron increases to $^{+4.9\%}_{-6.8\%}$ and becomes larger than for NNLL₂.

	Tevatron	LHC ($\sqrt{s} = 7$ TeV)	LHC ($\sqrt{s} = 14$ TeV)
NLL ₂	{+5.5%, -7.4%}	{+11.7%, -8.9%}	{+11.6%, -8.0%}
NNLO _{app}	{+3.8%, -4.9%}	{+7.7%, -7.4%}	{+8.6%, -7.7%}
NNLL ₂	{+4.2%, -6.5%}	{+4.6%, -4.6%}	{+4.5%, -4.1%}

Table 4: Relative error of NLL₂, NNLO_{app} and NNLL₂ at the LHC. Scale uncertainty, resummation ambiguity and the error from the NNLO constant are added in quadrature.

	Channel	Tevatron	LHC ($\sqrt{s} = 7$ TeV)
NNLO _{app}	$q\bar{q}$	$6.18^{+0.21+0.07}_{-0.27-0.07} \left\{ \begin{array}{l} +3.6\% \\ -4.5\% \end{array} \right\}$	$28.7^{+2.6+0.4}_{-2.9-0.4} \left\{ \begin{array}{l} +9.2\% \\ -10.2\% \end{array} \right\}$
NNLL ₂	$q\bar{q}$	$6.31^{+0.23+0.12+0.07}_{-0.41-0.20-0.07} \left\{ \begin{array}{l} +4.3\% \\ -7.3\% \end{array} \right\}$	$28.7^{+2.4+0.3+0.4}_{-3.0-1.9-0.4} \left\{ \begin{array}{l} +8.5\% \\ -12.5\% \end{array} \right\}$
NNLO _{app}	gg	$0.95^{+0.10+0.02}_{-0.09-0.02} \left\{ \begin{array}{l} +10.7\% \\ -9.7\% \end{array} \right\}$	$133.2^{+17.4+4.3}_{-13.8-4.3} \left\{ \begin{array}{l} +13.5\% \\ -10.9\% \end{array} \right\}$
NNLL ₂	gg	$0.98^{+0.02+0.12+0.02}_{-0.08-0.05-0.02} \left\{ \begin{array}{l} +12.6\% \\ -9.8\% \end{array} \right\}$	$134.7^{+8.2+3.6+4.3}_{-12.5-3.9-4.3} \left\{ \begin{array}{l} +7.4\% \\ -10.2\% \end{array} \right\}$
NNLL ₂ ($\beta_{\text{cut}} = 0.54$)	gg	$0.99^{+0.06+0.05+0.02}_{-0.08-0.06-0.02} \left\{ \begin{array}{l} +8.1\% \\ -10.3\% \end{array} \right\}$	$134.7^{+8.2+3.6+4.3}_{-12.5-3.9-4.3} \left\{ \begin{array}{l} +7.4\% \\ -10.2\% \end{array} \right\}$

Table 5: Results for the $q\bar{q}$ - and gg -channel, Method 2, $m_t = 173.3$ GeV, all numbers in pb. The errors refer to scale variation, resummation ambiguity (for NNLL₂ only) and the NNLO constant term. The numbers in brackets denote the total relative error. Unless stated otherwise, the default values of β_{cut} , Eq. (4.15), are used.

than at the level of the hadronic cross section as in Method 1. Threshold logarithms are resummed locally rather than in an average sense in the region above β_{cut} , while problems related to very small soft scales for small β are avoided. The sensitivity to the precise value of β_{cut} is moderate and included in our error estimate. In Section 5 we use this method as our default implementation.

4.3 Effect of Coulomb resummation

In this section we would like to comment on the size of the bound-state contributions and Coulomb resummation, which were not (or only partially) included in previous works on $t\bar{t}$ threshold resummation.

Toponium-like bound states may form below the nominal production threshold due to the strong Coulomb attraction in the colour-singlet channel. In practice, the bound-states are smeared into a broad resonance due to the rapid $t \rightarrow bW$ decay. For an inclusive observable such as the total cross section the resonance effect can be computed by neglecting the top decay width and summing instead over the series of would-be toponium bound-state poles in the Coulomb Green function. The technical aspects are discussed in detail in Appendix B. In Table 6 we show the corresponding contribution to the cross section, denoted by BS, which are always included in the NNLL results we present. The first error denotes the sum in quadrature of scale and resummation uncertainties, determined as from Method 2, and the second one the PDF+ α_s error. The bound-state contributions, which contribute first at $O(\alpha_s^5)$, are rather small and make up less than 0.5% of the total cross section. The large theoretical error might be due to the more singular behaviour of the convolution of the bound-state correction with the soft function and the PDFs (c.f. (B.6)), which makes the cross section more sensitive to variations of μ_f and k_s .

Next, we discuss the effects due to the resummation of Coulomb corrections in the continuum ($E > 0$). To switch off the Coulomb effects in the resummation formula, we set the Coulomb function (2.11) in Eq. 2.1 to its first-order term in the expansion in α_s (see (A.1)),

$$J_R^{\text{triv}}(E) = \frac{m_t^2}{2\pi} \sqrt{\frac{E}{m_t}} . \quad (4.16)$$

We then consider the quantities

$$\begin{aligned} \delta\text{Cb}_1 &= \sigma^{\text{NNLL}_1} - \sigma_{\text{triv}}^{\text{NNLL}_1} , \\ \delta\text{Cb}_2 &= \sigma^{\text{NNLL}_2} - \sigma_{\text{triv}}^{\text{NNLL}_2} , \end{aligned} \quad (4.17)$$

where σ^{NNLL_i} denotes the total resummed cross section with the full Coulomb function (but excluding bound-state effects), matched according to prescription (4.1) or (4.2), and $\sigma_{\text{triv}}^{\text{NNLL}_i}$ the analogous quantity for the trivial potential function (4.16). In this case, the expansion of $\sigma_{\text{triv}}^{\text{NNLL}}$ to NLO or NNLO order is subtracted in the matching prescriptions (4.1) or (4.2). As a consequence of the matching to the fixed-order results, δCb_1 contains only terms of order α_s^4 or higher. In particular, it contains all the purely Coulomb contributions, and the interference of Coulomb corrections with hard and soft terms, at NNLO. δCb_2 contains only terms of order α_s^5 or higher, and gives a measure of the effect of Coulomb resummation beyond NNLO.

In Table 6 we show the central values for δCb_1 and δCb_2 . We do not show errors, which are large, due to $\delta\text{Cb}_{1,2}$ being defined as a difference. From the numbers in the table, it is clear that the dominant effect of Coulomb resummation is accounted for by the terms already included in NNLO_{app} , which coincide with the difference $\delta\text{Cb}_1 - \delta\text{Cb}_2$. They give a non-negligible correction at both Tevatron ($\sim 2\%$) and LHC ($\sim 1 - 2\%$). Beyond NNLO, Coulomb corrections, and their interference with soft and hard resummation, is very small ($\lesssim 0.5\%$), as can be inferred from the numbers for δCb_2 .

	Tevatron	LHC ($\sqrt{s} = 7$ TeV)	LHC ($\sqrt{s} = 14$ TeV)
BS	$0.014^{+0.011+0.005}_{-0.009-0.004}$	$0.67^{+0.33+0.12}_{-0.31-0.10}$	$3.1^{+1.7+0.5}_{-1.6-0.4}$
δCb_1	-0.140	2.81	7.8
δCb_2	-0.052	0.13	-0.3

Table 6: Bound-state and Coulomb contributions for $m_t = 173.3$ GeV, Method 2. All numbers in pb.

4.4 Comparison to other NNLO_{app} and NNLL predictions

Previous results for the total top cross section beyond NLO and NLL [40,66] use theoretical input equivalent to the NNLO_{app} result discussed in the present paper (and presented in detail in the subsequent section), but the complete NNLL threshold resummation (including Coulomb effects) performed here is new.

There exists a complementary approach to resummation, which is based on resumming logarithms in various kinematical limits different from the partonic threshold $\beta \rightarrow 0$ such as pair invariant mass (PIM) kinematics [37,38] to compute the invariant mass distribution, and one-particle inclusive (1PI) kinematics [41,42] for rapidity and transverse-momentum distributions. Results for the total cross section are then obtained by integrating PIM or 1PI differential cross sections, and do not include the higher-order Coulomb corrections, which, as discussed in section 4.3, amounts to an effect of -0.13 pb at the Tevatron and $+3.5$ pb ($+11$ pb) at the LHC with $\sqrt{s} = 7$ TeV ($\sqrt{s} = 14$ TeV). On the other hand, these calculations keep certain sets of power-suppressed terms in β that can be non-negligible, since the total cross section is dominated by contributions with $\beta > 0.3$. Therefore these approaches complement our treatment using the partonic threshold limit, and differences in the predictions can indicate systematical uncertainties of resummation. In Table 7 we compare the results from these approaches, which are either based on NNLO_{app} expansions or on NNLL resummations to ours.

The approximations based on 1PI and PIM kinematics are themselves subject to large ambiguities, analogous to the ambiguity between $E = \sqrt{\hat{s}} - 2m_t$ and $m_t\beta^2$ in the threshold limit. In [38,42] it is argued by comparison to the known fixed-order NLO results that a particular form of the singular distributions arising in the SCET-based resummation formalism is preferred over those used conventionally (e.g. [17,41]). This ambiguity between the conventional 1PI approximation and the 1PI_{SCET} implementation of [42] is reflected in the different predictions in the first two rows of Table 7. It is interesting to note that these kinematical ambiguities appear to be larger in 1PI and PIM kinematics than in the threshold approximation where we only found a small ambiguity (c.f. Table 3).

From the results in Table 7 it is seen that our results agree within the quoted errors with those of Kidonakis [41] in 1PI kinematics. While the tension with the predictions of Ahrens et. al. [38,42] is larger, the results for the LHC agree within the given errors, if the

		Tevatron	LHC ($\sqrt{s} = 7$ TeV)	LHC ($\sqrt{s} = 14$ TeV)
NNLO _{app} ^{1PI}	(Ref. [41])	7.08 ^{+0.20} _{-0.24}	163 ⁺⁷ ₋₅	920 ⁺⁶⁰ ₋₃₉
NNLO _{app} ^{1PI_{SCET}}	(Ref. [42])	6.63 ^{+0.00} _{-0.27}	155 ⁺³ ₋₂	851 ⁺²⁵ ₋₅
NNLO _{app} ^{PIM_{SCET}}	(Ref. [38])	6.62 ^{+0.05} _{-0.40}	155 ⁺⁸ ₋₈	860 ⁺⁴⁶ ₋₄₃
NNLL ^{1PI_{SCET}}	(Ref. [42])	6.55 ^{+0.16} _{-0.14}	150 ⁺⁷ ₋₇	824 ⁺⁴¹ ₋₄₄
NNLL ^{PIM_{SCET}}	(Ref. [38])	6.46 ^{+0.18} _{-0.19}	147 ⁺⁷ ₋₆	811 ⁺⁴⁵ ₋₄₂
NNLL ₂	this work	7.22 ^{+0.31} _{-0.47}	163 ⁺⁷ ₋₈	896 ⁺⁴⁰ ₋₃₇

Table 7: Comparison to previous NNLO_{app} and NNLL predictions for the central value $\mu_f = m_t$ and MSTW08NNLO PDFs, all numbers in pb. In the results of [41] $m_t = 173$ GeV, in those of [38, 42] $m_t = 173.1$ GeV. Only theory errors, excluding PDF and α_s errors, are shown. The NNLL₂ theory errors from table 2 have been added in quadrature.

size of the Coulomb corrections included in our results is taken into account. The size of the theory uncertainties quoted by the different groups are comparable at the LHC (except for the very small error assigned to NNLO_{app}^{1PI_{SCET}}), however our theory error includes an estimate of the missing NNLO constant and the resummation ambiguities, which are not included by the other groups. At the Tevatron, the agreement with the results of [38, 42] is worse, in particular for the resummed results. In this case our estimate of the theory error is more conservative than that of the other groups.¹⁰ The larger discrepancies between results obtained using different kinematical approximations might again point to a worse behaviour of the threshold approximation for the quark-antiquark channel dominant at the Tevatron, as discussed already at the end of Section 4.2.

5 Detailed numerical results

In this section we present numerical results for the combined NNLL resummation of soft and Coulomb effects for the total $t\bar{t}$ cross section at hadron colliders. This requires a choice of the parton distribution functions used in the convolution of the partonic cross section with the parton luminosity. Available fits for PDFs at NNLO accuracy are the sets of

¹⁰The quoted results from [41] for the Tevatron include an independent variation of μ_f and μ_r while the NNLO_{app} results from [38, 42] set $\mu_f = \mu_r$. Adding separate variations of both scales in quadrature and averaging the 1PI_{SCET} and PIM_{SCET} kinematics, Ahrens et.al. [70] recently obtained a slightly increased error estimated $\sigma_{t\bar{t}}^{\text{NNLO}_{\text{app}}} = 6.63^{+0.07}_{-0.41}$ pb. It is interesting to note that the difference between the two kinematics is larger for the resummed cross sections than for the NNLO_{app}-results combined in the prediction from [70].

MSTW2008NNLO [64], JR09 [71], ABKM09 [72], HERAPDF1.0 [73] and NNPDF2.1 [74]. Recent discussions of the impact of the differences among the different PDF fits on the top-pair cross section can be found in [74, 75], where it was shown that the MSTW and NNPDF sets yield consistent results, whereas there are larger differences between the other sets, partly due to different values of the strong coupling constant obtained by the different groups. For our results we use the MSTW2008NNLO PDF sets at 90% confidence level and the associated value of the strong coupling constant [64],

$$\alpha_s(M_Z^2) = 0.1171_{-0.0034}^{+0.0034}. \quad (5.1)$$

Besides numbers for the NNLL cross section, we also present the NLO result [11, 65] and NNLO_{app}, which adds to NLO the threshold expansion¹¹ of the NNLO correction [36] (see Appendix C for a summary of the analytical expressions) to illustrate the significance of higher-order results. For NLO we use the NLO PDFs and the associated value $\alpha_s(M_Z^2) = 0.1202_{-0.0039}^{+0.0032}$. In all three cases, we determine the joint PDF+ α_s uncertainty using the method described in [69]. Following [46] the theoretical uncertainty of the fixed-order NLO and NNLO_{app} approximations is determined by setting the central values of the renormalization and factorization scales, $\{\tilde{\mu}_r, \tilde{\mu}_f\}$, to m_t and varying both scales simultaneously in the interval $[\tilde{\mu}_i/2, 2\tilde{\mu}_i]$, imposing the additional constraint $1/2 \leq \mu_r/\mu_f \leq 2$.

For the NNLL resummed cross section we choose the β -dependent soft scale (4.12), (4.13), and the matching condition (4.2), denoting the corresponding result by NNLL₂. The error estimate follows the procedure detailed in Section 4.2. The errors from scale variation and the resummation ambiguities are added in quadrature, while the uncertainty from variation of the unknown NNLO constant is given as a separate error both for NNLL₂ and NNLO_{app}. The default value of the pole mass of the top is chosen as $m_t = 173.3$ GeV [76]. Results for $m_t = 165 \dots 180$ GeV are given in Table 9 for Tevatron, and in Tables 11 and 12 for LHC. In Sections 5.1 and 5.2 we also compare our results to recent measurements at Tevatron and LHC, while in Section 5.3 we illustrate the impact on the extraction of the top mass from measurements of the cross section.

5.1 Tevatron

The cross section results for Tevatron kinematics are summarized in Table 8. The difference between NNLL₂ and NLO amounts to about 8% of the NLO result. This correction is an interplay of genuine resummation effects, which amount to about 12% of the NLO result, and of switching from NLO to NNLO PDFs, which lowers the NLO cross section from the value given in the table to 6.46 pb. As evident from Table 8, the bulk of the resummation corrections are accounted for by the fixed-order soft and Coulomb terms at $\mathcal{O}(\alpha_s^4)$ (NNLO_{app}), which give a 9.5% correction to the NLO result, though higher-order

¹¹Note that we apply a strict threshold approximation for NNLO_{app}, i.e. we discard all terms scaling as $\mathcal{O}(\alpha_s^2\beta^0)$ or higher with respect to the leading Born cross section. Consequently, our central value for NNLO_{app} differs, albeit slightly, from the one obtained e.g. using HATHOR, [66], since there $\mathcal{O}(\alpha_s^2\beta^2)$ terms from the gq -channel are included. Furthermore, terms of the form $\text{const.} \times \ln(\mu_f/m_t)$, although known exactly at NNLO, are not included, in the spirit of a strict threshold expansion.

NLO	NNLO _{app}	NNLL ₂
6.68 ^{+0.36+0.51} _{-0.75-0.45}	7.06 ^{+0.25+0.10+0.69} _{-0.33-0.10-0.53}	7.22 ^{+0.29+0.10+0.71} _{-0.46-0.10-0.55}

Table 8: The total top-pair cross section (in pb) for $m_t = 173.3$ GeV at the Tevatron. The first set of errors refers to scale variation (scale variation+resummation ambiguities for NNLL₂), the last to PDF+ α_s error. The second set of errors for NNLO_{app}/NNLL₂ arises from variations of the unknown NNLO constant term.

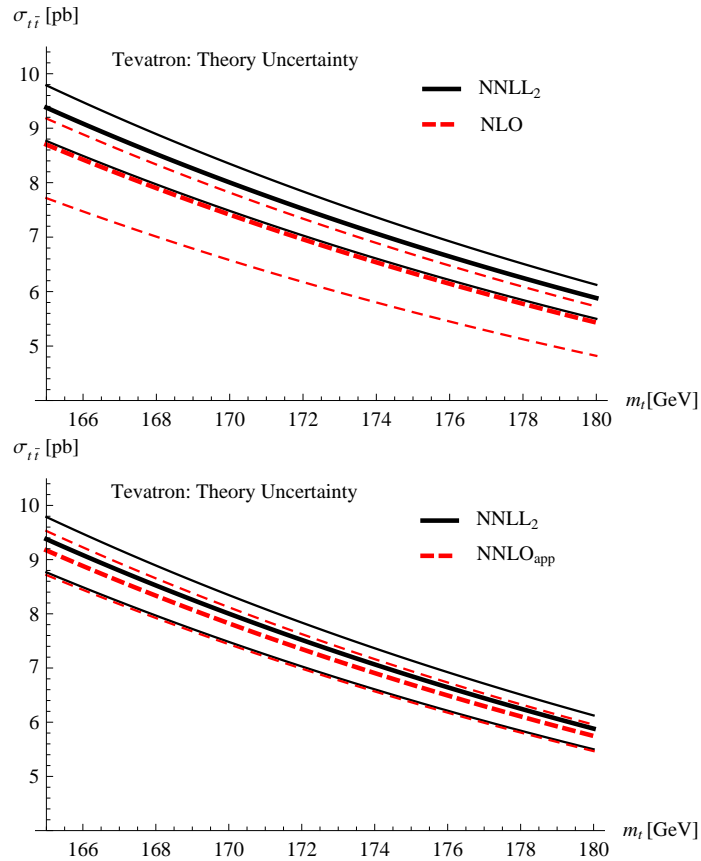


Figure 3: Dependence of the total cross section on the top mass at the Tevatron. The bands denote the total theory uncertainty, i.e. the sum (in quadrature) of the scale and resummation ambiguities, and the estimate of the NNLO constant but not the PDF + α_s error.

Table 9: Total cross sections in pb at the Tevatron for $m_t = 165 \dots 180$ GeV. The errors denote the scale variation (scale variation+resummation ambiguities for NNLL₂), the NNLO constant variation (for NNLO_{app} and NNLL₂) and the PDF+ α_s error.

m_t [GeV]	NLO	NNLO _{app}	NNLL ₂
165	8.70 ^{+0.48+0.66} _{-0.98-0.61}	9.17 ^{+0.33+0.13+0.93} _{-0.44-0.13-0.71}	9.38 ^{+0.39+0.13+0.96} _{-0.60-0.13-0.73}
166	8.42 ^{+0.46+0.64} _{-0.95-0.58}	8.88 ^{+0.32+0.13+0.89} _{-0.42-0.13-0.68}	9.08 ^{+0.37+0.13+0.92} _{-0.58-0.13-0.71}
167	8.16 ^{+0.45+0.62} _{-0.92-0.56}	8.60 ^{+0.31+0.12+0.86} _{-0.41-0.12-0.66}	8.80 ^{+0.36+0.12+0.89} _{-0.56-0.12-0.68}
168	7.90 ^{+0.43+0.60} _{-0.89-0.54}	8.33 ^{+0.30+0.12+0.83} _{-0.39-0.12-0.63}	8.52 ^{+0.35+0.12+0.86} _{-0.54-0.12-0.66}
169	7.65 ^{+0.42+0.58} _{-0.86-0.52}	8.07 ^{+0.29+0.11+0.80} _{-0.38-0.11-0.61}	8.26 ^{+0.34+0.11+0.83} _{-0.53-0.11-0.64}
170	7.41 ^{+0.41+0.56} _{-0.84-0.51}	7.82 ^{+0.28+0.11+0.78} _{-0.37-0.11-0.59}	8.00 ^{+0.32+0.11+0.80} _{-0.51-0.11-0.61}
171	7.18 ^{+0.39+0.54} _{-0.81-0.49}	7.58 ^{+0.27+0.11+0.75} _{-0.36-0.11-0.57}	7.76 ^{+0.31+0.11+0.77} _{-0.49-0.11-0.59}
172	6.96 ^{+0.38+0.53} _{-0.78-0.47}	7.35 ^{+0.26+0.10+0.72} _{-0.35-0.10-0.55}	7.52 ^{+0.30+0.10+0.75} _{-0.48-0.10-0.57}
173	6.74 ^{+0.37+0.51} _{-0.76-0.46}	7.12 ^{+0.25+0.10+0.70} _{-0.34-0.10-0.53}	7.29 ^{+0.29+0.10+0.72} _{-0.46-0.10-0.55}
174	6.54 ^{+0.36+0.50} _{-0.74-0.44}	6.91 ^{+0.24+0.09+0.67} _{-0.32-0.09-0.51}	7.07 ^{+0.28+0.09+0.70} _{-0.45-0.09-0.53}
175	6.34 ^{+0.34+0.48} _{-0.71-0.42}	6.70 ^{+0.23+0.09+0.65} _{-0.31-0.09-0.49}	6.85 ^{+0.27+0.09+0.67} _{-0.44-0.09-0.52}
176	6.14 ^{+0.33+0.47} _{-0.69-0.41}	6.49 ^{+0.22+0.09+0.63} _{-0.30-0.09-0.48}	6.64 ^{+0.26+0.09+0.65} _{-0.42-0.09-0.50}
177	5.96 ^{+0.32+0.45} _{-0.67-0.40}	6.30 ^{+0.22+0.09+0.61} _{-0.30-0.09-0.46}	6.44 ^{+0.26+0.09+0.63} _{-0.41-0.09-0.48}
178	5.78 ^{+0.31+0.44} _{-0.65-0.38}	6.11 ^{+0.21+0.08+0.59} _{-0.29-0.08-0.45}	6.25 ^{+0.25+0.08+0.61} _{-0.40-0.08-0.46}
179	5.60 ^{+0.30+0.43} _{-0.63-0.37}	5.92 ^{+0.20+0.08+0.57} _{-0.28-0.08-0.43}	6.06 ^{+0.24+0.08+0.59} _{-0.39-0.08-0.45}
180	5.43 ^{+0.29+0.42} _{-0.61-0.36}	5.75 ^{+0.19+0.08+0.55} _{-0.27-0.08-0.42}	5.88 ^{+0.23+0.08+0.57} _{-0.37-0.08-0.43}

contributions (from NNLO_{app} to NNLL₂) amount to a non-negligible 3.5%. The total theoretical error of the cross section is reduced at both NNLO_{app} and NNLL₂ compared to the NLO result, and amounts to $\{+4.2\%, -6.5\%\}$ for the NNLL₂ result, and $\{+3.8\%, -4.9\%\}$ for NNLO_{app}. As discussed in Section 4.2, the counter-intuitive increase of the uncertainty of the resummed result compared to the fixed-order NNLO is related to the behaviour of the quark-antiquark induced partonic subprocess. Interestingly, the relative PDF+ α_s uncertainty increases when going from NLO to NNLO_{app}/NNLL₂, an effect which is also observed at the LHC and has been found in [75] as well. The ambiguity arising from the unknown constant (second error) is small compared to the scale, resummation and PDF+ α_s uncertainties, which dominate the total error at NNLL₂.

The dependence of the total cross section on m_t is plotted in Figure 3 and given explicitly in Table 9. The relative theoretical errors in the mass range $m_t = 165 \dots 180$ GeV differ

\sqrt{s}	NLO	NNLO _{app}	NNLL ₂
7	158.1 ^{+19.5+13.9} _{-21.2-13.1}	161.1 ^{+11.4+4.7+15.2} _{-10.9-4.7-14.5}	162.6 ^{+5.7+4.7+15.4} _{-5.9-4.7-14.7}
14	884 ⁺¹⁰⁷⁺⁶⁵ ₋₁₀₆₋₅₈	891 ⁺⁷¹⁺²⁸⁺⁶⁴ ₋₆₃₋₂₈₋₆₃	896 ⁺²⁹⁺²⁸⁺⁶⁵ ₋₂₄₋₂₈₋₆₄

Table 10: Predictions for the total cross section (in pb) for $m_t = 173.3$ GeV at the LHC. The errors are defined as in Table 8.

only on the permille level from those for $m_t = 173.3$ GeV, while the PDF+ α_s uncertainty decreases slightly for larger masses, resulting in a practically constant overall uncertainty for NNLL₂ of $^{+11.1\%}$ _{-10.2%} at $m_t = 165$ GeV and $^{+10.5\%}$ _{-9.7%} at $m_t = 180$ GeV.

The NNLL₂ results are in good agreement with measurements performed at the Tevatron. The D0 experiment obtains $\sigma_{t\bar{t}} = 7.56^{+0.63}_{-0.56}$ pb from combining measurements of the dilepton and lepton plus jets final states with up to 5.6fb^{-1} of data [4]. The CDF collaboration quotes $\sigma_{t\bar{t}} = 7.50^{+0.48}_{-0.48}$ pb from a combination [2] of the dilepton, the lepton plus jets and the all-hadronic channel using up to 4.6fb^{-1} of data. A value of $\sigma_{t\bar{t}} = 7.70^{+0.52}_{-0.52}$ pb has been obtained from a measurement of the ratio of the top-pair and Z -boson production cross sections [1]. In these measurements a top mass $m_t = 172.5$ GeV has been used in the kinematical reconstruction of the top-events.

5.2 LHC

Our results for the LHC with centre-of-mass energies $\sqrt{s} = 7$ and 14 TeV are shown in Table 10. In Figure 4 we plot the dependence on \sqrt{s} of the NNLL₂ cross section. The difference between the NNLL₂ and NLO results is smaller than at Tevatron, and amounts to 3% (1%) at $\sqrt{s} = 7$ TeV ($\sqrt{s} = 14$ TeV). Again, the genuine effect of resummation is partly hidden by the switch to NNLO PDFs for the resummed results. Using NNLO PDFs for the NLO result would yield 148.9 pb and 837 pb for the NLO cross section at 7 and 14 TeV, which differ from the NNLL₂ results by 9% and 7%, respectively. As for the Tevatron, the bulk of the corrections beyond NLO come from the $\mathcal{O}(\alpha_s^2)$ terms, with higher order contributions at the 1% level.

The total theoretical error is largely reduced from NLO to NNLO_{app}, and from NNLO_{app} to NNLL₂ as seen from Table 10. For NNLL₂ it amounts to a $\{+4.5\%, -4.6\%$ residual uncertainty at $\sqrt{s} = 7$ TeV, and $\{+4.5\%, -4.1\%$ at $\sqrt{s} = 14$ TeV. Contrary to the Tevatron, the uncertainty arising from the variation of the unknown constant is comparable to the remaining theoretical error. This is a consequence of our estimate $|C_{pp',R}^{(2)\text{est.}}| = (C_{pp',R}^{(1)})^2$, see Eq. (4.9), which gives larger values at LHC, where the gg channel is dominant. At NNLL₂ the dominant source of uncertainty is the PDF+ α_s error, which is $\pm 9\%$. The total relative uncertainty, given by the sum in quadrature of all sources of error, is reduced from $\pm 15.5\%$ (NLO) to approximately $\pm 10.5\%$ (NNLL₂) at 7 TeV. A similar picture holds for 14 TeV, with a smaller total relative error, $\pm 8.5\%$.

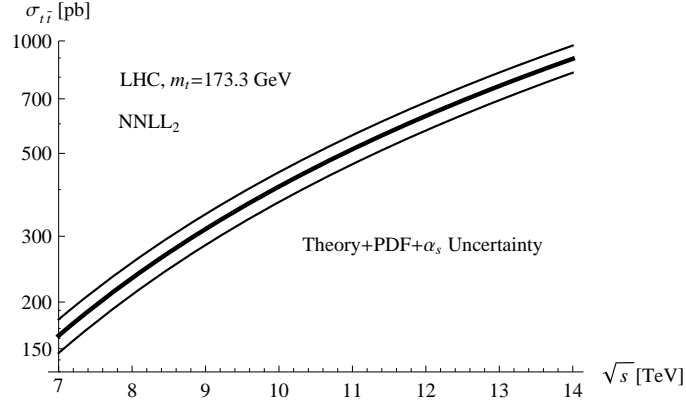


Figure 4: Dependence of the total cross section on \sqrt{s} at the LHC. The central line is obtained with our NNLL₂ prediction, while the band corresponds to the sum (in quadrature) of theory and PDF+ α_s errors.

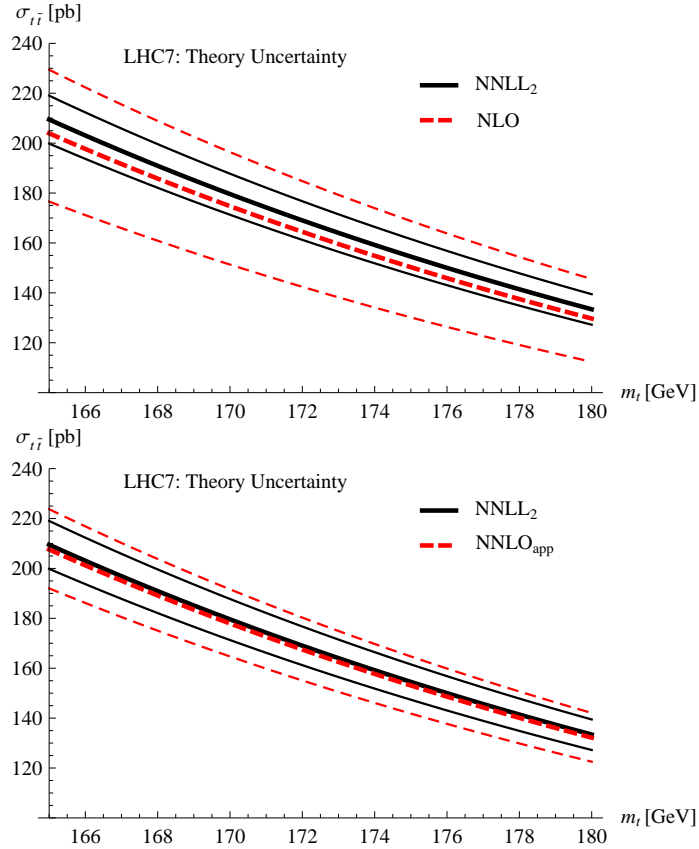


Figure 5: Dependence of the total cross section on the mass at the LHC with $\sqrt{s} = 7$ TeV. The bands denote the total theory uncertainty, i.e. the sum (in quadrature) of the scale and resummation ambiguities, and the estimate of the NNLO constant but not the PDF + α_s error.

Table 11: Total cross sections in pb at the LHC ($\sqrt{s} = 7$ TeV) for $m_t = 165 \dots 180$ GeV. The errors denote the scale variation (scale variation+resummation ambiguities for NNLL₂), the NNLO constant variation (for NNLO_{app} and NNLL₂) and the PDF+ α_s error.

m_t [GeV]	NLO	NNLO _{app}	NNLL ₂
165	203.9 ^{+25.5+17.8} _{-27.4-16.7}	207.6 ^{+15.0+6.1+19.3} _{-14.3-6.1-18.6}	209.5 ^{+7.3+6.1+19.6} _{-7.5-6.1-18.8}
166	197.7 ^{+24.7+17.3} _{-26.5-16.2}	201.2 ^{+14.5+5.9+18.8} _{-13.9-5.9-18.0}	203.1 ^{+7.1+5.9+19.0} _{-7.3-5.9-18.2}
167	191.6 ^{+23.9+16.8} _{-25.7-15.7}	195.1 ^{+14.0+5.7+18.2} _{-13.4-5.7-17.5}	196.9 ^{+6.9+5.7+18.5} _{-7.1-5.7-17.7}
168	185.8 ^{+23.1+16.3} _{-24.9-15.3}	189.2 ^{+13.5+5.5+17.7} _{-13.0-5.5-17.0}	190.9 ^{+6.7+5.5+17.9} _{-6.9-5.5-17.2}
169	180.2 ^{+22.4+15.8} _{-24.2-14.9}	183.5 ^{+13.1+5.4+17.2} _{-12.6-5.4-16.5}	185.2 ^{+6.5+5.4+17.4} _{-6.7-5.4-16.7}
170	174.7 ^{+21.7+15.3} _{-23.4-14.4}	177.9 ^{+12.7+5.2+16.7} _{-12.2-5.2-16.0}	179.6 ^{+6.3+5.2+16.9} _{-6.5-5.2-16.2}
171	169.5 ^{+21.0+14.9} _{-22.7-14.0}	172.6 ^{+12.3+5.0+16.2} _{-11.8-5.0-15.6}	174.2 ^{+6.1+5.0+16.5} _{-6.3-5.0-15.8}
172	164.4 ^{+20.3+14.5} _{-22.0-13.6}	167.5 ^{+11.9+4.9+15.8} _{-11.4-4.9-15.1}	169.0 ^{+6.0+4.9+16.0} _{-6.1-4.9-15.3}
173	159.6 ^{+19.7+14.0} _{-21.4-13.3}	162.5 ^{+11.5+4.7+15.4} _{-11.0-4.7-14.7}	164.0 ^{+5.8+4.7+15.6} _{-6.0-4.7-14.9}
174	154.8 ^{+19.1+13.6} _{-20.7-12.9}	157.7 ^{+11.1+4.5+14.9} _{-10.7-4.5-14.3}	159.2 ^{+5.6+4.5+15.1} _{-5.8-4.5-14.4}
175	150.3 ^{+18.5+13.3} _{-20.1-12.5}	153.1 ^{+10.8+4.4+14.5} _{-10.4-4.4-13.9}	154.5 ^{+5.5+4.4+14.7} _{-5.6-4.4-14.0}
176	145.9 ^{+17.9+12.9} _{-19.5-12.2}	148.6 ^{+10.4+4.3+14.1} _{-10.0-4.3-13.5}	150.0 ^{+5.3+4.3+14.3} _{-5.5-4.3-13.6}
177	141.6 ^{+17.4+12.5} _{-19.0-11.9}	144.3 ^{+10.1+4.1+13.7} _{-9.7-4.1-13.1}	145.6 ^{+5.2+4.1+13.9} _{-5.3-4.1-13.3}
178	137.5 ^{+16.9+12.2} _{-18.4-11.5}	140.1 ^{+9.8+4.0+13.4} _{-9.4-4.0-12.7}	141.4 ^{+5.0+4.0+13.5} _{-5.2-4.0-12.9}
179	133.5 ^{+16.3+11.8} _{-17.9-11.2}	136.1 ^{+9.5+3.9+13.0} _{-9.2-3.9-12.4}	137.4 ^{+4.9+3.9+13.2} _{-5.0-3.9-12.5}
180	129.7 ^{+15.9+11.5} _{-17.3-10.9}	132.2 ^{+9.2+3.8+12.6} _{-8.9-3.8-12.0}	133.4 ^{+4.7+3.8+12.8} _{-4.9-3.8-12.2}

The dependence of the cross section on m_t for $\sqrt{s} = 7$ TeV in different approximations is plotted in Figure 5. Additionally, numerical results for $m_t = 165 \dots 180$ GeV for NLO, NNLO_{app} and NNLL₂ at the LHC can be found in Tables 11 and 12. As for the Tevatron, the relative theory error is constant to a good accuracy in the considered mass interval, while the PDF+ α_s error increases slightly, resulting in a practically constant overall uncertainty ranging from $^{+10.4\%}_{-10.0\%}$ to $^{+10.6\%}_{-10.3\%}$ at $\sqrt{s} = 7$ TeV and from $^{+8.4\%}_{-8.2\%}$ to $^{+8.6\%}_{-8.3\%}$ at $\sqrt{s} = 14$ TeV.

Recently the LHC collaborations presented measurements of the total $t\bar{t}$ cross section that approach the experimental accuracy of the Tevatron. Utilizing kinematic information of lepton plus jets events, the ATLAS experiment obtains [5] $\sigma_{t\bar{t}} = 179.0 \pm 9.8(\text{stat+syst}) \pm 6.6(\text{lumi}) = 179.0 \pm 11.8$ pb using up to 0.7fb^{-1} of data, while the CMS collaboration obtains [6] $\sigma_{t\bar{t}} = 154 \pm 17(\text{stat+syst}) \pm 6(\text{lumi})$ pb from a combination of lepton plus jet

Table 12: Total cross sections in pb at the LHC ($\sqrt{s} = 14$ TeV) for $m_t = 165 \dots 180$ GeV. The errors denote the scale variation (scale variation+resummation ambiguities for NNLL₂), the NNLO constant variation (for NNLO_{app} and NNLL₂) and the PDF+ α_s error.

m_t [GeV]	NLO	NNLO _{app}	NNLL ₂
165	1111 ⁺¹³⁶⁺⁸² ₋₁₃₃₋₇₃	1118 ⁺⁹¹⁺³⁶⁺⁸⁰ ₋₈₀₋₃₆₋₇₈	1124 ⁺³⁶⁺³⁶⁺⁸⁰ ₋₃₀₋₃₆₋₇₉
166	1080 ⁺¹³²⁺⁸⁰ ₋₁₂₉₋₇₁	1087 ⁺⁸⁸⁺³⁵⁺⁷⁷ ₋₇₈₋₃₅₋₇₆	1093 ⁺³⁵⁺³⁵⁺⁷⁸ ₋₂₉₋₃₅₋₇₇
167	1051 ⁺¹²⁸⁺⁷⁸ ₋₁₂₆₋₆₉	1057 ⁺⁸⁶⁺³⁴⁺⁷⁵ ₋₇₆₋₃₄₋₇₄	1064 ⁺³⁴⁺³⁴⁺⁷⁶ ₋₂₈₋₃₄₋₇₅
168	1022 ⁺¹²⁴⁺⁷⁶ ₋₁₂₂₋₆₇	1029 ⁺⁸³⁺³³⁺⁷³ ₋₇₃₋₃₃₋₇₂	1035 ⁺³³⁺³³⁺⁷⁴ ₋₂₇₋₃₃₋₇₃
169	994 ⁺¹²¹⁺⁷³ ₋₁₁₉₋₆₅	1001 ⁺⁸¹⁺³²⁺⁷² ₋₇₁₋₃₂₋₇₁	1007 ⁺³²⁺³²⁺⁷² ₋₂₇₋₃₂₋₇₁
170	967 ⁺¹¹⁷⁺⁷¹ ₋₁₁₆₋₆₃	974 ⁺⁷⁹⁺³¹⁺⁷⁰ ₋₆₉₋₃₁₋₆₉	979 ⁺³¹⁺³¹⁺⁷⁰ ₋₂₆₋₃₁₋₆₉
171	941 ⁺¹¹⁴⁺⁷⁰ ₋₁₁₃₋₆₂	948 ⁺⁷⁶⁺³⁰⁺⁶⁸ ₋₆₇₋₃₀₋₆₇	953 ⁺³¹⁺³⁰⁺⁶⁹ ₋₂₅₋₃₀₋₆₈
172	916 ⁺¹¹¹⁺⁶⁸ ₋₁₁₀₋₆₀	922 ⁺⁷⁴⁺²⁹⁺⁶⁶ ₋₆₅₋₂₉₋₆₅	928 ⁺³⁰⁺²⁹⁺⁶⁶ ₋₂₅₋₂₉₋₆₆
173	892 ⁺¹⁰⁸⁺⁶⁶ ₋₁₀₇₋₅₈	898 ⁺⁷²⁺²⁸⁺⁶⁴ ₋₆₄₋₂₈₋₆₄	903 ⁺²⁹⁺²⁸⁺⁶⁵ ₋₂₄₋₂₈₋₆₄
174	868 ⁺¹⁰⁵⁺⁶⁴ ₋₁₀₄₋₅₇	874 ⁺⁷⁰⁺²⁸⁺⁶³ ₋₆₂₋₂₈₋₆₂	879 ⁺²⁸⁺²⁸⁺⁶³ ₋₂₃₋₂₈₋₆₃
175	845 ⁺¹⁰²⁺⁶³ ₋₁₀₁₋₅₅	851 ⁺⁶⁸⁺²⁷⁺⁶¹ ₋₆₀₋₂₇₋₆₀	856 ⁺²⁷⁺²⁷⁺⁶² ₋₂₃₋₂₇₋₆₁
176	823 ⁺⁹⁹⁺⁶¹ ₋₉₈₋₅₄	829 ⁺⁶⁶⁺²⁶⁺⁶⁰ ₋₅₈₋₂₆₋₅₉	834 ⁺²⁷⁺²⁶⁺⁶⁰ ₋₂₂₋₂₆₋₅₉
177	801 ⁺⁹⁶⁺⁵⁹ ₋₉₆₋₅₃	807 ⁺⁶⁴⁺²⁵⁺⁵⁸ ₋₅₇₋₂₅₋₅₇	812 ⁺²⁶⁺²⁵⁺⁵⁹ ₋₂₂₋₂₅₋₅₈
178	780 ⁺⁹⁴⁺⁵⁸ ₋₉₃₋₅₁	786 ⁺⁶²⁺²⁵⁺⁵⁷ ₋₅₅₋₂₅₋₅₆	791 ⁺²⁵⁺²⁵⁺⁵⁷ ₋₂₁₋₂₅₋₅₇
179	760 ⁺⁹¹⁺⁵⁶ ₋₉₁₋₅₀	766 ⁺⁶¹⁺²⁴⁺⁵⁵ ₋₅₄₋₂₄₋₅₅	770 ⁺²⁵⁺²⁴⁺⁵⁶ ₋₂₁₋₂₄₋₅₅
180	741 ⁺⁸⁹⁺⁵⁵ ₋₈₉₋₄₉	746 ⁺⁵⁹⁺²³⁺⁵⁴ ₋₅₂₋₂₃₋₅₃	751 ⁺²⁴⁺²³⁺⁵⁵ ₋₂₀₋₂₃₋₅₄

and dileptonic decay channels, using 0.036fb^{-1} . Both measurements are in agreement with our predictions within the uncertainties.

5.3 Top-quark mass determination

The ATLAS experiment also extracted the top mass from the measurement of the total cross section [9] by comparing the NNLO_{app} prediction of [7] to the cross section measured using different top-mass values in the kinematical reconstruction of the events. With 35pb^{-1} of data and an experimental cross section $\sigma_{t\bar{t}} = 186.3 \text{ pb} \pm 5\%(\text{stat}) \pm 12\%(\text{syst}) \pm 3\%(\text{lumi})$ for the reference top-mass $m_t = 172.5$ GeV, the ATLAS collaboration obtained the value $m_t = 166.4_{-7.3}^{+7.8}$ GeV for the pole mass. With a similar procedure, the D0 collaboration obtained the pole mass [8] $m_t = 167.5_{-4.7}^{+5.2}$ GeV from the cross section measurement

at the Tevatron.

It is interesting to speculate how the central value and the accuracy of the mass determination will change with the improved statistical accuracy of the latest LHC measurements and our NNLL₂ predictions. Following the method described in [9] we define a likelihood function

$$f(m_t) = \int f_{\text{th}}(\sigma|m_t) \cdot f_{\text{exp}}(\sigma|m_t) d\sigma, \quad (5.2)$$

where f_{th} is a normalized Gaussian distribution centred on the theoretical prediction of the cross section, having a width equal to the total error of the theory prediction

$$f_{\text{th}}(\sigma|m_t) = \frac{1}{\sqrt{2\pi}\Delta\sigma_{t\bar{t}}^{\text{th}}(m_t)} \exp\left[-\frac{(\sigma - \sigma_{t\bar{t}}^{\text{th}}(m_t))^2}{2(\Delta\sigma_{t\bar{t}}^{\text{th}}(m_t))^2}\right]. \quad (5.3)$$

f_{exp} is defined in a similar way, with the central value and width of the Gaussian given by the measured value of the cross section, $\sigma_{t\bar{t}}^{\text{exp}}(m_t)$, and the total experimental error, $\Delta\sigma_{t\bar{t}}^{\text{exp}}(m_t)$. The top-quark mass is then extracted from the maximum of the likelihood function (5.2), with the error obtained from the 68% area around the maximum.

The theoretical cross section $\sigma_{t\bar{t}}^{\text{th}}(m_t)$ is obtained using the numbers for the NNLL₂ approximation given in Table 11, interpolated by a function of the form

$$\sigma_{t\bar{t}}^{\text{th}}(m_t) = \left(\frac{172.5}{m_t}\right)^4 (c_0 + c_1(m_t - 172.5) + c_2(m_t - 172.5)^2 + c_3(m_t - 172.5)^3) \text{ pb}, \quad (5.4)$$

where all the masses are given in GeV. The total theory error is obtained by summing in quadrature the scale, resummation and the NNLO-constant uncertainties. For the PDF+ α_s uncertainty, the 68% CL set was used in the ATLAS note [9] and added linearly to the theory error. We account for this by rescaling our PDF+ α_s error. Furthermore, when the errors in the positive and negative directions differ from each other, the maximum of the two values is used. For the coefficients in the fit (5.4) we find $c_0 = 166.496 \pm 7.706 \pm 7.464$, $c_1 = -(1.15093 \pm 0.05687 \pm 0.03741)$, $c_2 = (5.06265 \pm 0.15147 \pm 0.15886) \times 10^{-3}$, $c_3 = (8.53722 \pm 12.1116 \pm (-3.19098)) \times 10^{-5}$ where the first error denotes the total theory error and the second the 68% CL PDF+ α_s error. Using the theoretical prediction provided by our NNLL₂ approximation, the measured $t\bar{t}$ cross section for the 35pb⁻¹ data set given in Table 1 of [9], and the extraction procedure described above, we obtain $m_t = 166.5_{-7.0}^{+8.0}$ GeV, which is in good agreement with the value extracted by the ATLAS collaboration using the NNLO_{app} result from [7].

For the more recent measurement obtained by ATLAS with improved statistics, the dependence of the measured cross section on the reference top mass was found to be well described by a linear fit [5]

$$\sigma_{t\bar{t}}^{\text{exp}}(m_t) = (411.9 - 1.35 m_t) \text{ pb} \quad (5.5)$$

in the interval $m_t = 160 - 190$ GeV. The mass dependence of both experimental and theoretical cross section is shown in Figure 6. Using the experimental result (5.5) and our

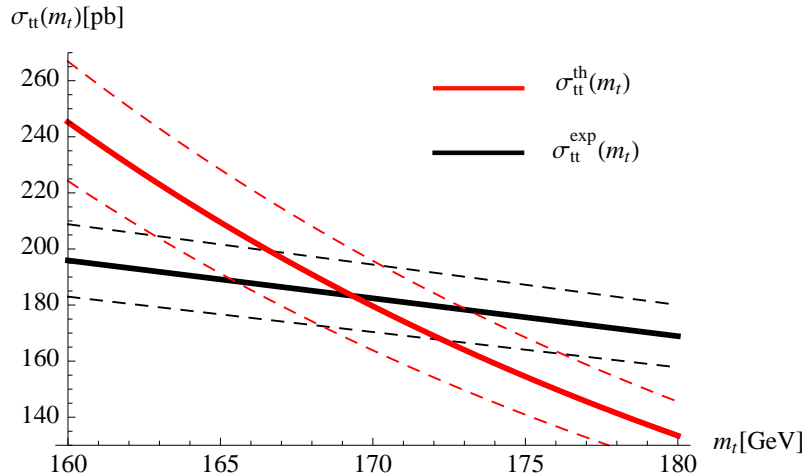


Figure 6: Mass dependence of the theoretical NNLL₂ cross section (red) and of the measured cross section (black), as obtained from Ref. [5]. The solid lines represent the central values, while the total uncertainties of the theoretical and experimental results, determined as explained in the text, are given by the external dashed lines.

theoretical prediction (5.4) for the evaluation of the likelihood function, we extract the pole mass

$$m_t = (169.8^{+4.9}_{-4.7}) \text{ GeV}, \quad (5.6)$$

where we have assumed that the total relative experimental error does not depend on m_t , and is equal to the relative error at the reference mass, $\Delta\sigma_{t\bar{t}}^{\text{exp}}/\sigma_{t\bar{t}}^{\text{exp}} = \pm 6.6\%$. It can be seen that the central value obtained from the 0.7 fb^{-1} data set is higher than the one obtained in [9], and the error is reduced to $\pm 3\%$. Also note that (5.6) agrees with the Tevatron measurement from direct reconstruction, $m_t = 173.3 \pm 1.1 \text{ GeV}$, at better than 1σ accuracy.

6 Conclusion

We calculated the total production cross section of top-antitop pairs at the Tevatron and the LHC based on a combined resummation of threshold logarithms and Coulomb corrections at NNLL accuracy, using the formalism developed in [34, 39]. We carefully assessed the ambiguities inherent in the resummation prescription, and adopted a new procedure for choosing the soft scale in the momentum-space approach to soft-gluon resummation in addition to the fixed scale advocated in [51, 52], obtaining consistent results with both methods within the estimated uncertainties. We also used the expansion of the NNLL result to obtain new approximate results at N³LO accuracy.

Our calculation accounts for bound-state corrections and higher-order Coulomb corrections not included in NNLL or NNLO_{app} calculations based on summing threshold

logarithms at fixed invariant mass [37, 38, 41, 42]. We find that the main effect of these corrections is included in the NNLO_{app} corrections obtained in [36], whereas the Coulomb corrections beyond NNLO are in the sub-percent range. The effect of NNLL resummation compared to the NNLO_{app} result of [36] is small, about 2% at the Tevatron and below 1% at the LHC. While this suggests that effects beyond NNLO are small, it is interesting to note that a larger effect is obtained by adding the partial N³LO results obtained from the expansion of the NNLL prediction. This might indicate that, from a certain perturbative order onwards, resummation should always be performed, even though the total effect is small.

Our results for a pole mass of $m_t = 173.3$ GeV, and using the MSTW08NNLO PDFs, are given by

$$\begin{aligned}
\sigma_{t\bar{t}}(\text{Tevatron}) &= (7.22_{-0.47-0.55}^{+0.31+0.71}) \text{ pb} \\
\sigma_{t\bar{t}}(\text{LHC}, \sqrt{s} = 7 \text{ TeV}) &= (162.6_{-7.6-14.7}^{+7.4+15.4}) \text{ pb} \\
\sigma_{t\bar{t}}(\text{LHC}, \sqrt{s} = 14 \text{ TeV}) &= (896_{-37-64}^{+40+65}) \text{ pb}
\end{aligned}
\tag{6.1}$$

where the first error denotes the combined theoretical uncertainty, including the scale uncertainty, estimates of resummation ambiguities and the unknown constant term in the threshold expansion of the NNLO cross section, and the second the PDF+ α_s uncertainty. The first error should be reduced once the full NNLO calculation of the top cross section is available. The reduction of the second one depends on the availability of a suitable reference cross section that depends on the gluon luminosity.

Using our NNLL₂ prediction and recent ATLAS measurements, we estimated that the top-quark mass could be extracted with an accuracy of ± 5 GeV from the currently available LHC data on the total cross section, and our result

$$m_t = (169.8_{-4.7}^{+4.9}) \text{ GeV}
\tag{6.2}$$

is compatible with the mass determination from direct reconstruction.

Acknowledgements

We would like to thank M. Cacciari, M. Mangano and A. Mitov for fruitful discussions during the completion of this manuscript. M.B. also thanks the Kavli Institute for Theoretical Physics at UC Santa Barbara for hospitality while part of this work was done. The work of M.B. and S.K. is supported by the DFG Sonderforschungsbereich/Transregio 9 ‘‘Computergestutzte Theoretische Teilchenphysik’’. P.F. acknowledges support by the ‘‘Stichting voor Fundamenteel Onderzoek der Materie (FOM)’’. This research was supported in part by the National Science Foundation under Grant No. PHY05-51164.

A NLO Coulomb function

The Coulomb Green functions at leading and next-to-leading order appearing in (2.11) read [53, 77]¹²

$$\begin{aligned}
 G_{C,R}^{(0)}(E) &= \frac{m_t^2}{4\pi} \left\{ -\sqrt{\frac{-E}{m_t}} - (-D_R)\alpha_s \left[-L_E - \frac{1}{2} + \hat{\psi}(1-\lambda) \right] \right\}, \\
 G_{C,R}^{(1)}(E) &= \frac{m_t^2}{16\pi^2} 4\pi(-D_R)\alpha_s \frac{\alpha_s}{4\pi} \left\{ a_1 [L_E + j_0] + \beta_0 [L_E^2 + 2j_0 L_E + j_1] \right\},
 \end{aligned} \tag{A.1}$$

where we have introduced the modified Euler psi function, $\hat{\psi}(x) = \gamma_E + \psi(x)$, the short-hands

$$\lambda = \frac{(-D_R)\alpha_s}{2\sqrt{-E}/m_t} \quad L_E = -\frac{1}{2} \ln \left(-\frac{4m_t E}{\mu^2} \right), \tag{A.2}$$

and the functions

$$j_0 = \lambda\psi'(1-\lambda) - \hat{\psi}(1-\lambda), \tag{A.3}$$

$$\begin{aligned}
 j_1 &= 4 {}_4F_3(1, 1, 1, 1; 2, 2, 1-\lambda; 1) + \lambda\psi''(1-\lambda) - 2\lambda\hat{\psi}(1-\lambda)\psi'(1-\lambda) \\
 &\quad - 3\psi'(1-\lambda) + \hat{\psi}(1-\lambda)^2 - \frac{\pi^2}{6}.
 \end{aligned} \tag{A.4}$$

The coefficients $\beta_0 = 11 - \frac{2}{3}n_l$ and $a_1 = \frac{31}{3} - \frac{10}{9}n_l$ ($n_l = 5$ light quarks) denote the first coefficient of the QCD beta-function and the one-loop correction to the Coulomb potential, respectively. The computation of the convolution (2.18) requires the numerical evaluation of the function j_1 and its derivatives for complex argument λ , which is explained in Section A.1. After the analytic continuation of the convolution of partonic cross sections with the parton luminosity, the potential function from (2.11) with Δ_{nC} set to one needs to be evaluated at $E = 0$, see (2.19). For the colour-singlet configuration ($D_R = -C_F$) this is given by

$$J_1(0) = \frac{m_t^2 C_F}{2\pi} \left\{ \pi\alpha_s - \alpha_s^2 \left[\frac{\beta_0}{2} \left(\ln \left(\frac{C_F \alpha_s m_t}{\mu} \right) + \gamma_E + 1 \right) - \frac{a_1}{4} \right] \right\} \quad (\text{for } \Delta_{\text{nC}} = 1). \tag{A.5}$$

The octet Coulomb function vanishes in this limit.

A.1 Evaluation of the NLO Coulomb function

The only non-trivial term in the NLO Coulomb function is the hypergeometric function ${}_4F_3$ in (A.4), which needs to be evaluated for complex λ . We define

$$F_{43} \equiv {}_4F_3(1, 1, 1, 1; 2, 2, N; 1) = \sum_{i=0}^{\infty} \frac{\Gamma(i+1)^3 \Gamma(N)}{\Gamma(i+2)^2 \Gamma(N+i)} \quad \text{with } N = 1 - \lambda. \tag{A.6}$$

¹²The expression for the NLO Coulomb-Green function obtained in [53] is quoted e.g. in [56].

By assuming that N is a positive integer, this sum is of the type which has been considered in [63], and can be expressed in terms of harmonic sums [78, 79],

$$F_{43} = (N - 1) \left\{ \zeta_3 - \zeta_2 S_1(N - 2) + S_3(N - 2) + S_1(N - 2) S_2(N - 2) - S_{2,1}(N - 2) \right\}. \quad (\text{A.7})$$

The single harmonic sums can be continued analytically to complex N by expressing them in terms of the ψ -function and its derivatives

$$S_1(N) = \psi(N + 1) + \gamma_E, \quad (\text{A.8})$$

$$S_a(N) = \frac{(-1)^{a-1}}{\Gamma(a)} \psi^{(a-1)}(N + 1) + \zeta_a, \quad \text{for } a \in \mathbb{N}, a \geq 2. \quad (\text{A.9})$$

The continuation of the nested harmonic sum $S_{2,1}(N)$ is well-defined as well and can be easily implemented, cf. e.g. [80, 81]. The result for F_{43} in terms of $\lambda \in \mathbb{C}$ then reads

$$F_{43} = \zeta_2 - S_2(-\lambda) - \lambda \left[\zeta_3 + S_3(-\lambda) - S_1(-\lambda) (\zeta_2 - S_2(-\lambda)) - S_{2,1}(-\lambda) \right]. \quad (\text{A.10})$$

The computation of the convolution (2.18) requires the numerical evaluation of derivatives of the NLO Coulomb function with respect to λ . Derivatives of the ψ -function and hence single harmonic sums are easily done, but the derivative of the $S_{2,1}$ requires more work. We use the package `HarmonicSums`, [82] for this task and obtain for the first derivative of F_{43}

$$\begin{aligned} \frac{d}{d\lambda} F_{43} = & -\lambda \frac{\zeta_2^2}{2} + \zeta_2 S_1(-\lambda) + \lambda \zeta_2 S_2(-\lambda) - S_1(-\lambda) S_2(-\lambda) \\ & - \lambda \frac{S_2^2(-\lambda)}{2} - 3S_3(-\lambda) - 2\lambda S_1(-\lambda) S_3(-\lambda) - 5\lambda \frac{S_4(-\lambda)}{2} \\ & + S_{2,1}(-\lambda) + 2\lambda S_{3,1}(-\lambda) + \zeta_3 + 2\lambda S_1(-\lambda) \zeta_3. \end{aligned} \quad (\text{A.11})$$

In (A.11) an additional nested harmonic sum appears, $S_{3,1}$, which can again be continued to complex λ using methods described in [80, 81].

B Bound-state corrections

Above the production threshold, $E > 0$, the potential function J_R is determined by the branch cut of the Coulomb Green function $G_{C,R}(E)$ along the real axis. Since we neglect the top decay width in the potential function, which is allowed when computing the total cross section, an imaginary part arises below threshold from isolated poles corresponding to $t\bar{t}$ bound-state production. The bound-state contribution to the potential function takes the form

$$J_R(E) = 2 \sum_{n=1}^{\infty} \delta(E - E_n) R_n \theta(-D_R), \quad E < 0 \quad (\text{B.1})$$

There are no bound states corrections when the Coulomb potential is repulsive ($D_R > 0$), as is the case in the colour-octet production channel, as indicated by the step function $\theta(-D_R)$. The leading-order bound-state energies and the residues read

$$E_n^{(0)} = -\frac{\alpha_s^2 D_R^2 m_t}{4n^2}, \quad R_n^{(0)} = \left(\frac{m_t(-D_{R\alpha})\alpha_s}{2n} \right)^3. \quad (\text{B.2})$$

While these expressions are sufficient for NLL resummation, the NLO Coulomb Green function shifts the energy and residue of the bound states to

$$E_n = E_n^{(0)} \left(1 + \frac{\alpha_s}{4\pi} e_1 \right), \quad R_n = R_n^{(0)} \left(1 + \frac{\alpha_s}{4\pi} \delta r_1 \right), \quad (\text{B.3})$$

with [83, 84]

$$e_1 = 2a_1 + 4\beta_0 \left[S_1(n) - \ln \left(\frac{m_t \alpha_s (-D_R)}{n\mu} \right) \right], \quad (\text{B.4})$$

$$\delta r_1 = 3a_1 + 2\beta_0 \left[S_1(n) + 2nS_2(n) - 1 - \frac{n\pi^2}{3} - 3 \ln \left(\frac{m_t \alpha_s (-D_R)}{n\mu} \right) \right]. \quad (\text{B.5})$$

The bound-state contributions to the partonic cross section are convoluted with the parton luminosity, similarly to the procedure discussed in Section 2.3. We mention here the relevant modifications. Recall that we do not apply the small correction Δ_{nC} in (2.11) to the already small bound-state contribution. Inserting (B.1) into the resummation formula and the convolution with the parton luminosity, we find

$$\begin{aligned} \sigma_{N_1 N_2 \rightarrow t\bar{t}X}^{BS} &= \sum_{p,p'=q,\bar{q},g} H_{pp'}^1(m_t, \mu) \int_0^1 d\tau L_{pp'}(\tau) \int_0^\infty d\omega J_1(E - \omega/2) W^1(\omega, \mu) \theta(\omega/2 - E) \\ &= \sum_{p,p'=q,\bar{q},g} \frac{2H_{pp'}^1(m_t, \mu)}{m_t} \exp[-4S(\mu_s, \mu_f) + 2a_W^1(\mu_s, \mu_f)] \tilde{s}^1(\partial_\eta, \mu_s) \frac{e^{-2\gamma_E \eta}}{\Gamma(2\eta)} \left(\frac{2m_t}{\mu_s} \right)^{2\eta} \\ &\quad \times \sum_n R_n \int_{\tau_n}^1 d\tau L_{pp'}(\tau) \left(\frac{E - E_n}{m_t} \right)^{2\eta-1}, \end{aligned} \quad (\text{B.6})$$

where $E = \sqrt{\tau s} - 2m_t$, and $H_{pp'}^1(m_t, \mu)$, $\tilde{s}^1(\partial_\eta, \mu_s)$ are the hard function and Laplace transform of the soft function for the singlet state. The integrals in the series have different lower integration limits, given by

$$\tau_n = \frac{1}{s} (2m_t + E_n)^2 < \tau_0 \equiv \frac{4m_t^2}{s}. \quad (\text{B.7})$$

For $\eta < 0$ the τ integrals have a non-integrable singularity at $\tau = \tau_n$ where $E - E_n \approx \sqrt{s/(4\tau_n)} (\tau - \tau_n)$. This is analogous to the convolution of the continuum cross section with the parton luminosity in Section 2.3. Following the method discussed there, the analytic continuation to negative η is constructed. However, here the integrand behaves

$\sim (\tau - \tau_n)^{2\eta-1}$ rather than $\sim (\tau - \tau_0)^{2\eta}$, so one further subtraction is required. To improve numerical stability we again introduce a parameter $\Lambda > \tau_0$ and split the integral into two integration domains,

$$\begin{aligned} \sum_n R_n \int_{\tau_n}^1 d\tau L_{pp'}(\tau) \left(\frac{E - E_n}{m_t} \right)^{2\eta-1} &= \sum_n R_n \left(\frac{\sqrt{s}}{m_t} \right)^{2\eta-1} \int_{\tau_n}^{\Lambda} d\tau L_{pp'}(\tau) (\sqrt{\tau} - \sqrt{\tau_n})^{2\eta-1} \\ &+ \int_{\Lambda}^1 d\tau L_{pp'}(\tau) \left(\frac{\sqrt{s}}{m_t} \right)^{2\eta-1} \sum_n R_n (\sqrt{\tau} - \sqrt{\tau_n})^{2\eta-1}. \end{aligned} \quad (\text{B.8})$$

In the second term we interchanged summation and integration. The second integral is free of singularities. Furthermore, the sum inside the integral is convergent. To isolate the singularities in the region $[\tau_n, \Lambda]$ we introduce the expansion of the integrand around $\tau = \tau_n$ as

$$\begin{aligned} \mathcal{T}_{\tau_n}^{(1)} [L_{pp'}(\tau)(\sqrt{\tau} - \sqrt{\tau_n})^{2\eta-1}] &= (4\tau_n)^{1/2-\eta} \left[L_{pp'}(\tau_n)(\tau - \tau_n)^{2\eta-1} \right. \\ &\quad \left. + \frac{4\tau_n L'_{pp'}(\tau_n) + (1 - 2\eta)L_{pp'}(\tau_n)}{4\tau_n} (\tau - \tau_n)^{2\eta} \right]. \end{aligned} \quad (\text{B.9})$$

Then, for $\eta < 0$, the integrals over the interval $[\tau_n, \Lambda]$ are analytically continued to $\eta > -1$ by the identity

$$\begin{aligned} \int_{\tau_n}^{\Lambda} d\tau L_{pp'}(\tau) (\sqrt{\tau} - \sqrt{\tau_n})^{2\eta-1} &= \int_{\tau_n}^{\Lambda} d\tau (1 - \mathcal{T}_{\tau_n}^{(1)}) [L_{pp'}(\tau)(\sqrt{\tau} - \sqrt{\tau_n})^{2\eta-1}] \\ &+ (4\tau_n)^{1/2-\eta} (\Lambda - \tau_n)^{2\eta} \left[\frac{L_{pp'}(\tau_n)}{2\eta} + \frac{4\tau_n L'_{pp'}(\tau_n) + (1 - 2\eta)L_{pp'}(\tau_n)}{4(1 + 2\eta)\tau_n} (\Lambda - \tau_n) \right]. \end{aligned} \quad (\text{B.10})$$

The poles at $\eta = 0, -1/2$ are now manifest and cancelled by the factor $1/\Gamma(2\eta)$ in (B.6). The remaining integral in (B.10) is singularity-free if $\eta > -1$, and can be computed numerically. This requires the numerical evaluation of the first derivative of the parton-luminosity functions, $L'_{pp'}$. The integral (B.10) can be continued to arbitrary negative values of η by performing more subtractions. However, for the applications presented in this paper, the continuation to $\eta > -1$ is sufficient. The convergence of the series in n , and the stability of the numerical integration, depend on the choice of the separation parameter Λ . We adopt $\Lambda = 1.002\tau_0$, and truncate the series over bound states at level $n_{\text{max}} = 100$.

C Fixed-order expansions

C.1 Expansion to $\mathcal{O}(\alpha_s^2)$

In this appendix we provide the NNLO corrections to the cross section (3.1) resulting from expanding the NNLL resummed result. The scale-independent terms for the three partonic

channels are given by

$$f_{q\bar{q}(8)}^{(2,0)} = \frac{3.60774}{\beta^2} + \frac{1}{\beta} (-140.368 \ln^2 \beta + 32.106 \ln \beta + 3.95105) + 910.222 \ln^4 \beta - 1315.53 \ln^3 \beta + 592.292 \ln^2 \beta + 528.557 \ln \beta + \tilde{f}_{q\bar{q}(8)}^{(2,0)}, \quad (\text{C.1})$$

$$f_{gg(1)}^{(2,0)} = \frac{230.896}{\beta^2} + \frac{1}{\beta} (2526.62 \ln^2 \beta + 1347.76 \ln \beta + 66.1114) + 4608. \ln^4 \beta - 249.2 \ln^3 \beta - 2385.73 \ln^2 \beta + 1600.47 \ln \beta + \tilde{f}_{gg(1)}^{(2,0)}, \quad (\text{C.2})$$

$$f_{gg(8)}^{(2,0)} = \frac{3.60774}{\beta^2} + \frac{1}{\beta} (-315.827 \ln^2 \beta - 89.5134 \ln \beta - 38.5162) + 4608 \ln^4 \beta - 2553.2 \ln^3 \beta - 322.996 \ln^2 \beta + 2799.24 \ln \beta + \tilde{f}_{gg(8)}^{(2,0)}. \quad (\text{C.3})$$

The terms shown explicitly are known exactly and have first been obtained fully in [36]. The functions $\tilde{f}_X^{(2,0)}$ are constant terms in the threshold expansion that are currently not known completely, since, for example, the two-loop hard functions contribute to them. At the NNLL level, they therefore show a residual dependence on the numerical factors k_i in the scale choices $\mu_s = k_s m_t \beta^2$, and $\mu_h = k_h m_t$. These terms are given by

$$\begin{aligned} \tilde{f}_{q\bar{q}(8)}^{\text{NNLL}(2,0)} &= -56.889 \ln^4 k_h + 240.692 \ln^3 k_h - 116.423 \ln^2 k_h - 456.803 \ln k_h \\ &\quad - 56.889 \ln^4 k_s - 164.441 \ln^3 k_s - 52.0528 \ln^2 k_s + 319.029 \ln k_s \\ &\quad + 49.7741, \end{aligned} \quad (\text{C.4})$$

$$\begin{aligned} \tilde{f}_{gg(1)}^{\text{NNLL}(2,0)} &= -288. \ln^4 k_h + 921.172 \ln^3 k_h - 8.19545 \ln^2 k_h - 1322.62 \ln k_h - 288. \ln^4 k_s \\ &\quad - 31.15 \ln^3 k_s + 1231. \ln^2 k_s + 1295.98 \ln k_s - 328.235, \end{aligned} \quad (\text{C.5})$$

$$\begin{aligned} \tilde{f}_{gg(8)}^{\text{NNLL}(2,0)} &= -288. \ln^4 k_h + 633.172 \ln^3 k_h + 543.378 \ln^2 k_h - 1109.7 \ln k_h - 288. \ln^4 k_s \\ &\quad - 319.15 \ln^3 k_s + 847.638 \ln^2 k_s + 1626.13 \ln k_s - 43.6962. \end{aligned} \quad (\text{C.6})$$

The factorization-scale dependent terms for the partonic channels are

$$f_{gg(1)}^{(2,1)} = \frac{1}{\beta} (403.557 - 2526.62 \ln \beta) - 9216 \ln^3 \beta + 3567.82 \ln^2 \beta + 2639.47 \ln \beta + \tilde{f}_{gg(1)}^{(2,1)}, \quad (\text{C.7})$$

$$f_{gg(1)}^{(2,2)} = 4608 \ln^2 \beta - 3563.96 \ln \beta + \tilde{f}_{gg(1)}^{(2,2)}, \quad (\text{C.8})$$

$$f_{gg(8)}^{(2,1)} = \frac{1}{\beta} (315.827 \ln \beta - 50.4446) - 9216 \ln^3 \beta + 5871.82 \ln^2 \beta - 25.2877 \ln \beta + \tilde{f}_{gg(8)}^{(2,1)}, \quad (\text{C.9})$$

$$f_{gg(8)}^{(2,2)} = f_{gg(1)}^{(2,2)}. \quad (\text{C.10})$$

In this case the constant terms are known exactly:

$$\tilde{f}_{q\bar{q}(8)}^{(2,1)} = 327.048, \quad \tilde{f}_{q\bar{q}(8)}^{(2,2)} = 385.383, \quad (\text{C.11})$$

$$\tilde{f}_{gg(1)}^{(2,1)} = -487.213, \quad \tilde{f}_{gg(1)}^{(2,2)} = -417.165, \quad (\text{C.12})$$

$$\tilde{f}_{gg(8)}^{(2,1)} = -283.914, \quad \tilde{f}_{gg(8)}^{(2,2)} = \tilde{f}_{gg(1)}^{(2,2)}. \quad (\text{C.13})$$

C.2 Expansion to $\mathcal{O}(\alpha_s^3)$

Here we provide those parts of the N³LO corrections to the cross section (3.1) that have not been given already in Section 3, i.e. the scale dependent terms $f_X^{(3,i)}$ for $i = 1, 2, 3$ and the NNLL approximations to the functions $\tilde{f}_X^{(3,i)}$, that are beyond the NNLL accuracy of the threshold expansion. The expressions that follow are generated from expanding the resummation formula as given in Eqs. (3.48) and (3.49) of [39] (appropriately adapted to the case of top-quark production).

Quark-antiquark channel. The scaling functions of the scale-dependent contributions in the N³LO expansion of the quark-antiquark production channel are given by

$$f_{q\bar{q}(8)}^{(3,1)} = \frac{1}{\beta^2} (-153.93 \ln \beta + 56.8546) + \frac{1}{\beta} (5989.02 \ln^3 \beta - 7733.19 \ln^2 \beta - 2669.2 \ln \beta) - 38836.1 \ln^5 \beta + 109310. \ln^4 \beta - 78403.7 \ln^3 \beta + \tilde{f}_{q\bar{q}(8)}^{(3,1)}, \quad (\text{C.14})$$

$$f_{q\bar{q}(8)}^{(3,2)} = \frac{1}{\beta} (-2994.51 \ln^2 \beta + 5287.18 \ln \beta) + 38836.1 \ln^4 \beta - 111164 \ln^3 \beta + \tilde{f}_{q\bar{q}(8)}^{(3,2)}, \quad (\text{C.15})$$

$$f_{q\bar{q}(8)}^{(3,3)} = -12945.4 \ln^3 \beta + \tilde{f}_{q\bar{q}(8)}^{(3,3)}, \quad (\text{C.16})$$

where all the terms shown explicitly are exact. These are the only terms included in the N³LO_B approximation, while the N³LO_A approximation includes in addition the NNLL approximation to the $\tilde{f}^{(3,i)}$ -functions. Most of the terms in these functions can only be predicted exactly from resummation beyond NNLL accuracy. At the NNLL level, they show a residual dependence on the numerical factors k_i in the scale choices $\mu_s = k_s m_t \beta^2$, $\mu_h = k_h m_t$ and $\mu_C = k_C m_t \beta$. For the quark-antiquark channel these functions read

$$\begin{aligned} \tilde{f}_{q\bar{q}(8)}^{\text{NNLL}(3,0)} = & \frac{1}{\beta} (773.485 \ln^2 k_C - 335.834 \ln k_C + 187.157 \ln^4 k_h - 791.846 \ln^3 k_h \\ & + 383.015 \ln^2 k_h + 1502.82 \ln k_h + 187.157 \ln^4 k_s + 81.5526 \ln^3 k_s \\ & - 1199.28 \ln^2 k_s - 2174.59 \ln k_s + 749.55) + \ln \beta (-2331.66 \ln k_C \\ & + 1172.51 \ln^4 k_h - 4960.79 \ln^3 k_h + 2399.53 \ln^2 k_h + 9414.94 \ln k_h \\ & + 4661.69 \ln^4 k_s + 4398.91 \ln^3 k_s - 27481 \ln^2 k_s - 60914.9 \ln k_s + 11370.2) \\ & + \ln^2 \beta (-2427.26 \ln^4 k_h + 10269.5 \ln^3 k_h - 4967.37 \ln^2 k_h \end{aligned}$$

$$\begin{aligned}
& -19490.3 \ln k_h - 2427.26 \ln^4 k_s - 7016.16 \ln^3 k_s - 2220.92 \ln^2 k_s \\
& + 13611.9 \ln k_s - 65560) - 404.543 \ln^6 k_h + 3730.45 \ln^5 k_h \\
& - 10015.2 \ln^4 k_h + 5148.7 \ln^3 k_h + 9150.36 \ln^2 k_h - 5460.36 \ln k_h \\
& + 404.543 \ln^6 k_s + 2917.1 \ln^5 k_s + 1022.1 \ln^4 k_s - 12319 \ln^3 k_s \\
& - 15042.1 \ln^2 k_s + 5890.83 \ln k_s + 702.307, \tag{C.17}
\end{aligned}$$

$$\begin{aligned}
\tilde{f}_{q\bar{q}(8)}^{\text{NNLL}(3,1)} &= \frac{2272.92}{\beta} - 38012.7 \ln^2 \beta + \ln \beta (2427.26 \ln^4 k_h - 10269.5 \ln^3 k_h \\
& + 4967.37 \ln^2 k_h + 19490.3 \ln k_h + 2427.26 \ln^4 k_s + 7016.16 \ln^3 k_s \\
& + 2220.92 \ln^2 k_s - 13611.9 \ln k_s + 67825.2) - 3323.77 \ln^4 k_h + 14062.6 \ln^3 k_h \\
& - 6802.08 \ln^2 k_h - 26436.3 \ln k_h - 3323.77 \ln^4 k_s - 5069.58 \ln^3 k_s \\
& + 12832 \ln^2 k_s + 36025.7 \ln k_s + 327.661, \tag{C.18}
\end{aligned}$$

$$\tilde{f}_{q\bar{q}(8)}^{\text{NNLL}(3,2)} = -\frac{1005.67}{\beta} + 78770 \ln^2 \beta - 3383.32 \ln \beta - 3697.7, \tag{C.19}$$

$$\tilde{f}_{q\bar{q}(8)}^{\text{NNLL}(3,3)} = 39223.6 \ln^2 \beta - 28867.1 \ln \beta + 1140.45. \tag{C.20}$$

Gluon fusion colour-singlet channel. The scaling functions for the factorization-scale dependent terms are

$$\begin{aligned}
f_{gg(1)}^{(3,1)} &= \frac{1}{\beta^2} (-22166 \ln \beta - 8283.49) + \frac{1}{\beta} (-242555 \ln^3 \beta - 51902.1 \ln^2 \beta + 217024 \ln \beta) \\
& - 442368 \ln^5 \beta + 300977 \ln^4 \beta + 563908 \ln^3 \beta + \tilde{f}_{gg(1)}^{(3,1)}, \tag{C.21}
\end{aligned}$$

$$f_{gg(1)}^{(3,2)} = \frac{1}{\beta} (121278 \ln^2 \beta - 58112.2 \ln \beta) + 442368 \ln^4 \beta - 448309 \ln^3 \beta + \tilde{f}_{gg(1)}^{(3,2)}, \tag{C.22}$$

$$f_{gg(1)}^{(3,3)} = -147456 \ln^3 \beta + \tilde{f}_{gg(1)}^{(3,3)}. \tag{C.23}$$

The NNLL approximations for the terms in the scaling functions not exactly known read

$$\begin{aligned}
\tilde{f}_{gg(1)}^{(3,0)} &= \frac{1}{\beta} (-6187.88 \ln^2 k_C + 2686.67 \ln k_C - 7579.86 \ln^4 k_h + 24244.3 \ln^3 k_h \\
& - 215.695 \ln^2 k_h - 34809.9 \ln k_h - 7579.86 \ln^4 k_s + 17787.4 \ln^3 k_s \\
& + 49075.2 \ln^2 k_s + 10292.7 \ln k_s - 14467) + \ln \beta (36589.2 \ln k_C \\
& - 2196.4 \ln^4 k_h + 7025.22 \ln^3 k_h - 62.5017 \ln^2 k_h - 10086.8 \ln k_h \\
& + 15467.6 \ln^4 k_s - 101709 \ln^3 k_s - 211987 \ln^2 k_s - 10792.4 \ln k_s + 112623.) \\
& + \ln^2 \beta (-27648 \ln^4 k_h + 88432.5 \ln^3 k_h - 786.763 \ln^2 k_h - 126971 \ln k_h \\
& - 27648 \ln^4 k_s - 2990.4 \ln^3 k_s + 118176 \ln^2 k_s + 124414 \ln k_s - 146090) \\
& - 4608 \ln^6 k_h + 27996.1 \ln^5 k_h - 42685.9 \ln^4 k_h - 17071.1 \ln^3 k_h
\end{aligned}$$

$$\begin{aligned}
& + 45365.4 \ln^2 k_h + 13255 \ln k_h + 4608 \ln^6 k_s + 6635.6 \ln^5 k_s - 62517.1 \ln^4 k_s \\
& - 79096.6 \ln^3 k_s + 37998.9 \ln^2 k_s + 37910.9 \ln k_s - 9739.8, \tag{C.24}
\end{aligned}$$

$$\begin{aligned}
\tilde{f}_{gg(1)}^{\text{NNLL}(3,1)} = & - \frac{29709.3}{\beta} - 618319 \ln^2 \beta + \ln \beta (27648 \ln^4 k_h - 88432.5 \ln^3 k_h \\
& + 786.763 \ln^2 k_h + 126971 \ln k_h + 27648 \ln^4 k_s + 2990.4 \ln^3 k_s \\
& - 118176 \ln^2 k_s - 124414 \ln k_s + 198168) - 17315.9 \ln^4 k_h + 55385.1 \ln^3 k_h \\
& - 492.747 \ln^2 k_h - 78953.1 \ln k_h - 17315.9 \ln^4 k_s + 49817.9 \ln^3 k_s \\
& + 146950 \ln^2 k_s + 48514.7 \ln k_s - 77934, \tag{C.25}
\end{aligned}$$

$$\tilde{f}_{gg(1)}^{\text{NNLL}(3,2)} = - \frac{43685.6}{\beta} - 297750 \ln^2 \beta + 322713 \ln \beta - 52925.9, \tag{C.26}$$

$$\tilde{f}_{gg(1)}^{\text{NNLL}(3,3)} = 206398 \ln^2 \beta + 10843.3 \ln \beta - 50289.8. \tag{C.27}$$

Gluon fusion colour-octet channel. The scaling functions for the factorization-scale dependent terms are

$$\begin{aligned}
f_{gg(8)}^{(3,1)} = & \frac{1}{\beta^2} (-346.343 \ln \beta - 129.429) + \frac{1}{\beta} (30319.4 \ln^3 \beta - 1092.09 \ln^2 \beta - 21802.5 \ln \beta) \\
& - 442368 \ln^5 \beta + 522161 \ln^4 \beta + 227359 \ln^3 \beta + \tilde{f}_{gg(8)}^{(3,1)}, \tag{C.28}
\end{aligned}$$

$$f_{gg(8)}^{(3,2)} = \frac{1}{\beta} (-15159.7 \ln^2 \beta + 7264.03 \ln \beta) + 442368 \ln^4 \beta - 558901 \ln^3 \beta + \tilde{f}_{gg(8)}^{(3,2)}, \tag{C.29}$$

$$f_{gg(8)}^{(3,3)} = - 147456 \ln^3 \beta + \tilde{f}_{gg(8)}^{(3,3)}. \tag{C.30}$$

The NNLL approximations for the terms in the scaling functions not exactly known read

$$\begin{aligned}
\tilde{f}_{gg(8)}^{\text{NNLL}(3,0)} = & \frac{1}{\beta} (773.485 \ln^2 k_C - 335.834 \ln k_C + 947.482 \ln^4 k_h - 2083.05 \ln^3 k_h \\
& - 1787.64 \ln^2 k_h + 3650.77 \ln k_h + 947.482 \ln^4 k_s - 1275.94 \ln^3 k_s \\
& - 6617.62 \ln^2 k_s - 4868.71 \ln k_s + 2424.05) + \ln^2 \beta (-27648 \ln^4 k_h \\
& + 60784.5 \ln^3 k_h + 52164.3 \ln^2 k_h - 106531 \ln k_h - 27648 \ln^4 k_s \\
& - 30638.4 \ln^3 k_s + 81373.3 \ln^2 k_s + 156108 \ln k_s - 347424) \\
& + \ln \beta (-2152.3 \ln k_C + 4715.6 \ln^4 k_h - 10367.3 \ln^3 k_h - 8897.06 \ln^2 k_h \\
& + 18169.8 \ln k_h + 22379.6 \ln^4 k_s - 78581.5 \ln^3 k_s - 289277 \ln^2 k_s - 205101 \ln k_s \\
& + 123426.) - 4608 \ln^6 k_h + 21084.1 \ln^5 k_h - 19739.3 \ln^4 k_h - 26067.8 \ln^3 k_h \\
& + 33695.1 \ln^2 k_h + 1303.32 \ln k_h + 4608 \ln^6 k_s + 13547.6 \ln^5 k_s - 50831.9 \ln^4 k_s \\
& - 118982 \ln^3 k_s - 16519.8 \ln^2 k_s + 62214.4 \ln k_s + 966.578, \tag{C.31}
\end{aligned}$$

$$\tilde{f}_{gg(8)}^{\text{NNLL}(3,1)} = \frac{5903.02}{\beta} - 748536 \ln^2 \beta + \ln \beta (27648 \ln^4 k_h - 60784.5 \ln^3 k_h$$

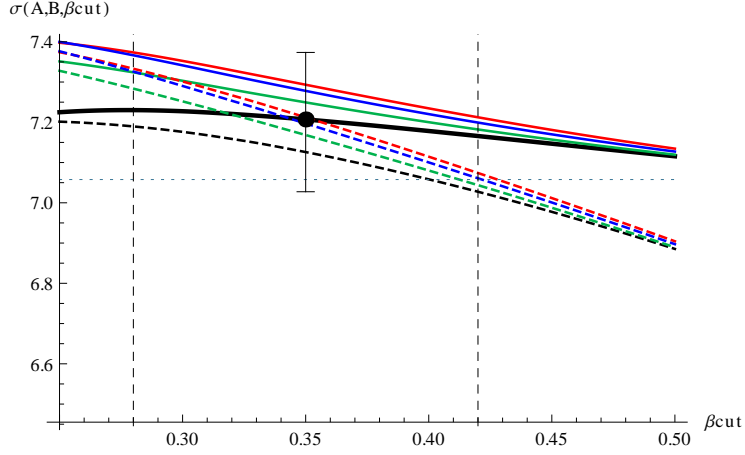


Figure 7: Determination of β_{cut} and the resulting ambiguity for the Tevatron with $k_s = 2$. The plot shows $\sigma_{t\bar{t}}(A_{<}, B_{>}, \beta_{\text{cut}})$ (in pb), as defined by convoluting (4.14) with the parton luminosity. Solid curves: $A_{<} = \text{NNLL}_2$, dashed curves $A_{<} = \text{NNLL}_1$, black curves: $B_{>} = \text{NNLL}_2$, red curves: $B_{>} = \text{NNLO}_{\text{app}}$, blue curves: $B_{>} = \text{N}^3\text{LO}_B$, green curves: $B_{>} = \text{N}^3\text{LO}_A$. The horizontal dotted line is the NNLO_{app} cross section, the x -axis intersects the y axis at the value of the NLO cross section. The point with the error bar is the central value of the cross section together with the error estimate, obtained by taking the envelope of the curves in the $\pm 20\%$ window around the default $\beta_{\text{cut}} = 0.35$, given by the vertical dashed lines.

$$\begin{aligned}
& -52164.3 \ln^2 k_h + 106531 \ln k_h + 27648 \ln^4 k_s + 30638.4 \ln^3 k_s \\
& -81373.3 \ln^2 k_s - 156108 \ln k_s + 399352) - 17315.9 \ln^4 k_h + 38069.2 \ln^3 k_h \\
& + 32670.3 \ln^2 k_h - 66151.5 \ln k_h - 17315.9 \ln^4 k_s + 32502.1 \ln^3 k_s \\
& + 162669 \ln^2 k_s + 137140 \ln k_s - 61943.1, \tag{C.32}
\end{aligned}$$

$$\tilde{f}_{gg(8)}^{\text{NNLL}(3,2)} = \frac{5460.7}{\beta} - 100578 \ln^2 \beta + 284537 \ln \beta - 88163.8, \tag{C.33}$$

$$\tilde{f}_{gg(8)}^{\text{NNLL}(3,3)} = \tilde{f}_{gg(1)}^{\text{NNLL}(3,3)}. \tag{C.34}$$

D Details of Method 2

We provide here the numerical details defining β_{cut} in Method 2, as discussed in Section 4.2, and the corresponding implementation at the NLL order. Figures 7 and 8 show the various approximations (4.14) for $k_s = 2$ at the Tevatron and at the LHC, respectively, together with the default β_{cut} and the 20%-window used in the estimate iii) of the resummation ambiguity. The plots show the expected behaviour: for increasing β_{cut} (and hence $\mu_s^<$) resummation becomes less effective and the difference between the two implementations used in the lower interval (the difference between solid and dashed lines of the same colour)

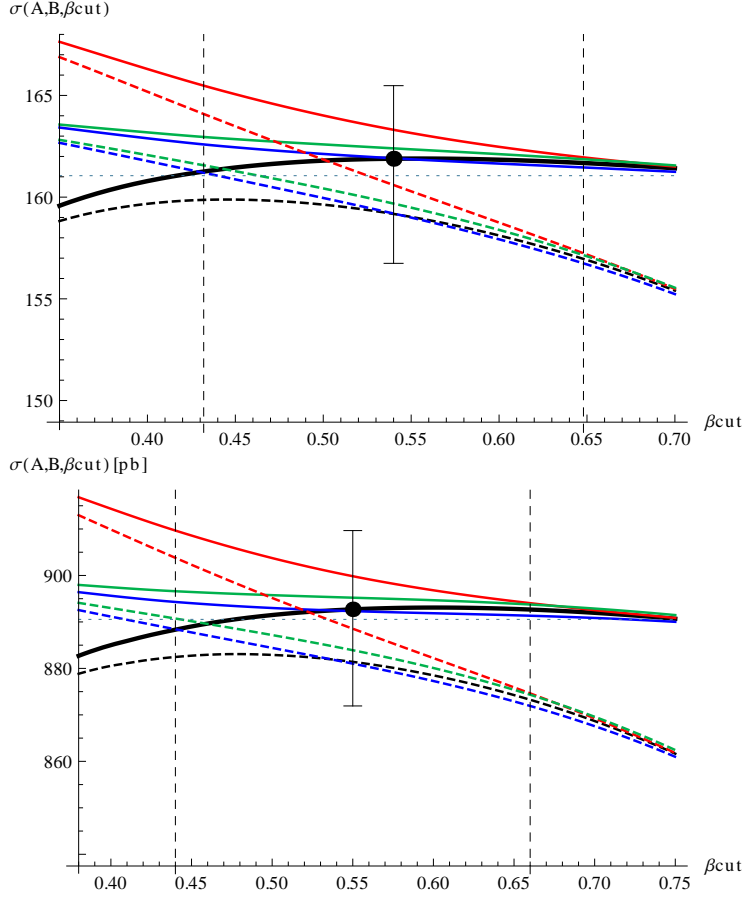


Figure 8: Determination of β_{cut} and the resulting ambiguity for the LHC with 7 TeV (above) and 14 TeV (below). The curves are the cross section $\sigma_{t\bar{t}}(A_{<}, B_{>}, \beta_{\text{cut}})$, with the various approximations defined as in Figure 7.

becomes dominant. For smaller β_{cut} the difference of the resummed cross section and perturbative expansions to different orders used in the upper interval (e.g. the difference among the solid lines of different colour) becomes sizeable, while the difference between the two NNLL implementations in the lower interval becomes negligible. Note that the default curve (the black solid line) depends only weakly on the precise value used for β_{cut} . The spread among the different approximations for varying β_{cut} by 20% leads to an uncertainty of $\sim 2.5\%$ for both Tevatron and LHC. This is the dominant contribution to our estimate of the resummation uncertainty. The criteria i) and ii) discussed in Section 4.2 both contribute uncertainties $\sim 1.5\%$ or smaller, cf. Table 3 .

Finally we also present the values of β_{cut} one obtains when varying k_s by a factor of 2 around its default value $k_s = 2$ for $m_t = 173.3$ GeV. We obtain

$$\begin{aligned}
\underline{k_s = 1} : \\
\beta_{\text{cut}}(\text{NNLL}) : & \quad 0.52 \text{ (Tevatron)}, & \quad 0.75 \text{ (LHC7)}, & \quad 0.79 \text{ (LHC14)}, \\
\mu_s^< = m_t \beta_{\text{cut}}^2 : & \quad 47 \text{ GeV (Tevatron)}, & \quad 97 \text{ GeV (LHC7)}, & \quad 108 \text{ GeV (LHC14)} .
\end{aligned} \tag{D.1}$$

$$\begin{aligned}
\underline{k_s = 4} : \\
\beta_{\text{cut}}(\text{NNLL}) : & \quad 0.23 \text{ (Tevatron)}, & \quad 0.33 \text{ (LHC7)}, & \quad 0.33 \text{ (LHC14)}, \\
\mu_s^< = 4m_t \beta_{\text{cut}}^2 : & \quad 37 \text{ GeV (Tevatron)}, & \quad 76 \text{ GeV (LHC7)}, & \quad 76 \text{ GeV (LHC14)}.
\end{aligned} \tag{D.2}$$

As one would expect, the corresponding soft scales $\mu_s^<$ lie not very far apart from each other for $k_s = 1, 2, 4$, Eq. (4.15) for $k_2 = 2$.

For resummation at NLL order, we determine β_{cut} anew, using the same prescription to minimize the spread between different cross sections (4.14) for the approximations $A_< \in \{\text{NLL}_1, \text{NLL}_2\}$ (defined in (4.3) and (4.4)) in the lower interval and $B_> \in \{\text{NLL}_2, \text{NLO}, \text{NLL-NNLO}_A, \text{NLL-NNLO}_B\}$ in the upper interval. Here, in analogy to the two N³LO approximations, NLL-NNLO_A denotes the expansion of the NLL corrections to order α_s^2 , keeping all the generated terms, while only those terms exactly reproduced at NLL accuracy (i.e. the terms $\alpha_s^2 \{ \frac{1}{\beta^2}, \frac{\ln^2 \beta}{\beta}, \frac{\ln \beta}{\beta}, \ln^4 \beta, \ln^3 \beta \}$) are kept in the NLL-NNLO_B approximation. With this prescription, the resulting β_{cut} -values at NLL for $k_s = 2$ are somewhat smaller than for NNLL resummation:

$$\beta_{\text{cut}}(\text{NLL}) : \quad 0.26 \text{ (Tevatron)}, \quad 0.32 \text{ (LHC7)}, \quad 0.32 \text{ (LHC14)} \tag{D.3}$$

The remaining uncertainties are estimated as for NNLL.

References

- [1] **CDF** Collaboration, T. Aaltonen *et al.*, *Phys. Rev. Lett.* **105** (2010) 012001, [arXiv:1004.3224](https://arxiv.org/abs/1004.3224) [hep-ex].
- [2] **CDF** Collaboration. Conference note 9913, 2009. http://www-cdf.fnal.gov/physics/new/top/confNotes/cdf9913_ttbarxs4invfb.ps.
- [3] **D0** Collaboration, V. M. Abazov *et al.*, [arXiv:1101.0124](https://arxiv.org/abs/1101.0124) [hep-ex].
- [4] **D0** Collaboration, V. M. Abazov *et al.*, [arXiv:1105.5384](https://arxiv.org/abs/1105.5384) [hep-ex].
- [5] **ATLAS** Collaboration. Conference note atlas-conf-2011-121, 2011. <https://atlas.web.cern.ch/Atlas/GROUPS/PHYSICS/CONFNOTES/ATLAS-CONF-2011-121/ATLAS-C>
- [6] **CMS** Collaboration, [arXiv:1108.3773](https://arxiv.org/abs/1108.3773) [hep-ex].
- [7] U. Langenfeld, S. Moch, and P. Uwer, *Phys. Rev.* **D80** (2009) 054009, [arXiv:0906.5273](https://arxiv.org/abs/0906.5273) [hep-ph].

- [8] **D0** Collaboration, V. M. Abazov *et al.*, [arXiv:1104.2887](#) [hep-ex].
- [9] **ATLAS** Collaboration. Conference note atlas-conf-2011-54, 2011.
<https://atlas.web.cern.ch/Atlas/GROUPS/PHYSICS/CONFNOTES/ATLAS-CONF-2011-054/ATLAS-C>
- [10] **CDF** Collaboration, T. Aaltonen *et al.*, [arXiv:1101.0034](#) [hep-ex].
- [11] P. Nason, S. Dawson, and R. K. Ellis, *Nucl. Phys.* **B303** (1988) 607.
- [12] E. Laenen, J. Smith, and W. L. van Neerven, *Nucl. Phys.* **B369** (1992) 543–599.
- [13] S. Catani, M. L. Mangano, P. Nason, and L. Trentadue,
Phys. Lett. **B378** (1996) 329–336, [arXiv:hep-ph/9602208](#).
- [14] E. L. Berger and H. Contopanagos, *Phys. Rev.* **D54** (1996) 3085–3113,
[arXiv:hep-ph/9603326](#).
- [15] N. Kidonakis, J. Smith, and R. Vogt, *Phys. Rev.* **D56** (1997) 1553–1570,
[arXiv:hep-ph/9608343](#).
- [16] R. Bonciani, S. Catani, M. L. Mangano, and P. Nason,
Nucl. Phys. **B529** (1998) 424–450, [arXiv:hep-ph/9801375](#).
- [17] N. Kidonakis, E. Laenen, S. Moch, and R. Vogt, *Phys. Rev.* **D64** (2001) 114001,
[arXiv:hep-ph/0105041](#).
- [18] M. Czakon, *Phys. Lett.* **B664** (2008) 307–314, [arXiv:0803.1400](#).
- [19] R. Bonciani, A. Ferroglia, T. Gehrmann, D. Maitre, and C. Studerus,
JHEP **07** (2008) 129, [arXiv:0806.2301](#).
- [20] R. Bonciani, A. Ferroglia, T. Gehrmann, and C. Studerus, *JHEP* **08** (2009) 067,
[arXiv:0906.3671](#).
- [21] J. G. Körner, Z. Merebashvili, and M. Rogal, *Phys. Rev.* **D77** (2008) 094011,
[arXiv:0802.0106](#).
- [22] C. Anastasiou and S. M. Aybat, *Phys. Rev.* **D78** (2008) 114006, [arXiv:0809.1355](#).
- [23] B. Kniehl, Z. Merebashvili, J. G. Körner, and M. Rogal,
Phys. Rev. **D78** (2008) 094013, [arXiv:0809.3980](#).
- [24] S. Dittmaier, P. Uwer, and S. Weinzierl, *Phys. Rev. Lett.* **98** (2007) 262002,
[arXiv:hep-ph/0703120](#).
- [25] R. Bonciani, A. Ferroglia, T. Gehrmann, A. Manteuffel, and C. Studerus,
JHEP **01** (2011) 102, [arXiv:1011.6661](#).
- [26] M. Czakon, *Nucl.Phys.* **B849** (2011) 250–295, [arXiv:1101.0642](#) [hep-ph].

- [27] I. Bierenbaum, M. Czakon, and A. Mitov, [arXiv:1107.4384 \[hep-ph\]](#).
- [28] N. Kidonakis, *Phys. Rev. Lett.* **102** (2009) 232003, [arXiv:0903.2561 \[hep-ph\]](#).
- [29] A. Mitov, G. Sterman, and I. Sung, *Phys. Rev.* **D79** (2009) 094015, [arXiv:0903.3241 \[hep-ph\]](#).
- [30] T. Becher and M. Neubert, *Phys. Rev.* **D79** (2009) 125004, [arXiv:0904.1021 \[hep-ph\]](#).
- [31] A. Ferroglia, M. Neubert, B. D. Pecjak, and L. L. Yang, *Phys. Rev. Lett.* **103** (2009) 201601, [arXiv:0907.4791 \[hep-ph\]](#).
- [32] A. Ferroglia, M. Neubert, B. D. Pecjak, and L. L. Yang, *JHEP* **11** (2009) 062, [arXiv:0908.3676 \[hep-ph\]](#).
- [33] A. Mitov, G. F. Sterman, and I. Sung, *Phys. Rev.* **D82** (2010) 034020, [arXiv:1005.4646](#).
- [34] M. Beneke, P. Falgari, and C. Schwinn, *Nucl. Phys.* **B828** (2010) 69–101, [arXiv:0907.1443 \[hep-ph\]](#).
- [35] M. Czakon, A. Mitov, and G. Sterman, *Phys. Rev.* **D80** (2009) 074017, [arXiv:0907.1790 \[hep-ph\]](#).
- [36] M. Beneke, M. Czakon, P. Falgari, A. Mitov, and C. Schwinn, *Phys. Lett.* **B690** (2010) 483–490, [arXiv:0911.5166 \[hep-ph\]](#).
- [37] V. Ahrens, A. Ferroglia, M. Neubert, B. D. Pecjak, and L. L. Yang, *Phys. Lett.* **B687** (2010) 331–337, [arXiv:0912.3375 \[hep-ph\]](#).
- [38] V. Ahrens, A. Ferroglia, M. Neubert, B. D. Pecjak, and L. L. Yang, *JHEP* **09** (2010) 097, [arXiv:1003.5827](#).
- [39] M. Beneke, P. Falgari, and C. Schwinn, *Nucl. Phys.* **B842** (2011) , [arXiv:1007.5414 \[hep-ph\]](#).
- [40] M. Beneke, P. Falgari, S. Klein, and C. Schwinn, *Nucl. Phys. Proc. Suppl.* **205-206** (2010) 20–24, [arXiv:1009.4011](#).
- [41] N. Kidonakis, *Phys. Rev.* **D82** (2010) 114030, [arXiv:1009.4935](#).
- [42] V. Ahrens, A. Ferroglia, M. Neubert, B. D. Pecjak, and L. L. Yang, [arXiv:1103.0550](#).
- [43] G. Sterman, *Nucl. Phys.* **B281** (1987) 310.
- [44] S. Catani and L. Trentadue, *Nucl. Phys.* **B327** (1989) 323.

- [45] S. Moch and P. Uwer, *Phys. Rev.* **D78** (2008) 034003, arXiv:0804.1476 [hep-ph].
- [46] M. Cacciari, S. Frixione, M. L. Mangano, P. Nason, and G. Ridolfi, *JHEP* **09** (2008) 127, arXiv:0804.2800 [hep-ph].
- [47] N. Kidonakis and R. Vogt, *Phys. Rev.* **D78** (2008) 074005, arXiv:0805.3844 [hep-ph].
- [48] K. Hagiwara, Y. Sumino, and H. Yokoya, *Phys. Lett.* **B666** (2008) 71–76, arXiv:0804.1014 [hep-ph].
- [49] Y. Kiyo, J. H. Kühn, S. Moch, M. Steinhauser, and P. Uwer, *Eur. Phys. J.* **C60** (2009) 375–386, arXiv:0812.0919 [hep-ph].
- [50] T. Becher and M. Neubert, *Phys. Rev. Lett.* **97** (2006) 082001, hep-ph/0605050.
- [51] T. Becher, M. Neubert, and B. D. Pecjak, *JHEP* **01** (2007) 076, hep-ph/0607228.
- [52] T. Becher, M. Neubert, and G. Xu, *JHEP* **07** (2008) 030, arXiv:0710.0680 [hep-ph].
- [53] M. Beneke, A. Signer, and V. A. Smirnov, *Phys. Lett.* **B454** (1999) 137–146, arXiv:hep-ph/9903260.
- [54] A. H. Hoang *et al.*, *Eur. Phys. J. direct* **C2** (2000) 1, arXiv:hep-ph/0001286.
- [55] A. H. Hoang, A. V. Manohar, I. W. Stewart, and T. Teubner, *Phys. Rev.* **D65** (2002) 014014, arXiv:hep-ph/0107144.
- [56] A. Pineda and A. Signer, *Nucl. Phys.* **B762** (2007) 67–94, arXiv:hep-ph/0607239.
- [57] W. Bernreuther, M. Fückler, and Z.-G. Si, *Phys. Rev.* **D74** (2006) 113005, arXiv:hep-ph/0610334.
- [58] J. H. Kühn, A. Scharf, and P. Uwer, *Eur. Phys. J.* **C51** (2007) 37–53, arXiv:hep-ph/0610335.
- [59] A. Denner, S. Dittmaier, S. Kallweit, and S. Pozzorini, *Phys. Rev. Lett.* **106** (2011) 052001, arXiv:1012.3975 [hep-ph].
- [60] G. Bevilacqua, M. Czakon, A. van Hameren, C. G. Papadopoulos, and M. Worek, *JHEP* **02** (2011) 083, arXiv:1012.4230 [hep-ph].
- [61] N. Kidonakis and G. Sterman, *Nucl. Phys.* **B505** (1997) 321–348, arXiv:hep-ph/9705234.
- [62] M. Czakon and A. Mitov, *Phys. Lett.* **B680** (2009) 154–158, arXiv:0812.0353 [hep-ph].

- [63] I. Bierenbaum, J. Blümlein, S. Klein, and C. Schneider, *Nucl.Phys.* **B803** (2008) 1–41, [arXiv:0803.0273 \[hep-ph\]](#).
- [64] A. D. Martin, W. J. Stirling, R. S. Thorne, and G. Watt, *Eur. Phys. J.* **C63** (2009) 189–285, [arXiv:0901.0002 \[hep-ph\]](#).
- [65] M. Czakon and A. Mitov, *Nucl. Phys.* **B824** (2010) 111–135, [arXiv:0811.4119 \[hep-ph\]](#).
- [66] M. Aliev *et al.*, *Comput. Phys. Commun.* **182** (2011) 1034–1046, [arXiv:1007.1327](#).
- [67] T. Gehrmann and E. Remiddi, *Comput.Phys.Commun.* **141** (2001) 296–312, [arXiv:hep-ph/0107173 \[hep-ph\]](#).
- [68] M. Bonvini, S. Forte, and G. Ridolfi, *Nucl. Phys.* **B847** (2011) 93–159, [arXiv:1009.5691 \[hep-ph\]](#).
- [69] A. D. Martin, W. J. Stirling, R. S. Thorne, and G. Watt, *Eur. Phys. J.* **C64** (2009) 653–680, [arXiv:0905.3531 \[hep-ph\]](#).
- [70] V. Ahrens, A. Ferroglia, B. D. Pecjak, and L. L. Yang, [arXiv:1105.5824 \[hep-ph\]](#).
- [71] P. Jimenez-Delgado and E. Reya, *Phys. Rev.* **D79** (2009) 074023, [arXiv:0810.4274 \[hep-ph\]](#).
- [72] S. Alekhin, J. Blümlein, S. Klein, and S. Moch, *Phys. Rev.* **D81** (2010) 014032, [arXiv:0908.2766 \[hep-ph\]](#).
- [73] **H1 and ZEUS** Collaboration, F. D. Aaron *et al.*, *JHEP* **01** (2010) 109, [arXiv:0911.0884 \[hep-ex\]](#).
- [74] **The NNPDF** Collaboration, R. D. Ball *et al.*, [arXiv:1107.2652 \[hep-ph\]](#).
- [75] G. Watt, [arXiv:1106.5788 \[hep-ph\]](#).
- [76] **CDF and D0** Collaboration, Tevatron Electroweak Working Group, [arXiv:1007.3178 \[hep-ex\]](#).
- [77] M. Beneke, [arXiv:hep-ph/9911490](#). Proceedings of the 8th International Symposium on Heavy Flavor Physics (Heavy Flavors 8), Southampton, England, 25-29 Jul 1999.
- [78] J. A. M. Vermaseren, *Int. J. Mod. Phys.* **A14** (1999) 2037–2076, [arXiv:hep-ph/9806280](#).
- [79] J. Blümlein and S. Kurth, *Phys. Rev.* **D60** (1999) 014018, [arXiv:hep-ph/9810241](#).
- [80] J. Blümlein, *Comput.Phys.Commun.* **180** (2009) 2218–2249, [arXiv:0901.3106 \[hep-ph\]](#).

- [81] S. Albino, *Phys.Lett.* **B674** (2009) 41–48, arXiv:0902.2148 [hep-ph].
- [82] J. Ablinger, arXiv:1011.1176 [math-ph].
- [83] A. Pineda and F. Yndurain, *Phys.Rev.* **D58** (1998) 094022, arXiv:hep-ph/9711287 [hep-ph].
- [84] M. Beneke, Y. Kiyo, and K. Schuller, *Nucl.Phys.* **B714** (2005) 67–90, arXiv:hep-ph/0501289 [hep-ph].